

AD 607642

AIR FORCE  
BALLISTIC MISSILE DIVISION  
TECHNICAL LIBRARY

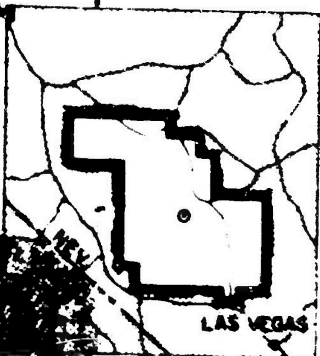
WT-1528



Document No. \_\_\_\_\_  
Copy No. \_\_\_\_\_

AEC Category: HEALTH AND SAFETY  
Military Category: \_\_\_\_\_

# OPERATION PLUMBBOB



NEVADA TEST SITE  
MAY-OCTOBER 1957

✓  
9

COPY	OF	Cost
HARD COPY	1	\$ 2.25
MICROFICHE	1	\$ 0.75

Project 26.4a

43+

## SURFACE MOTION FROM AN UNDERGROUND DETONATION

Issuance Date: March 31, 1960

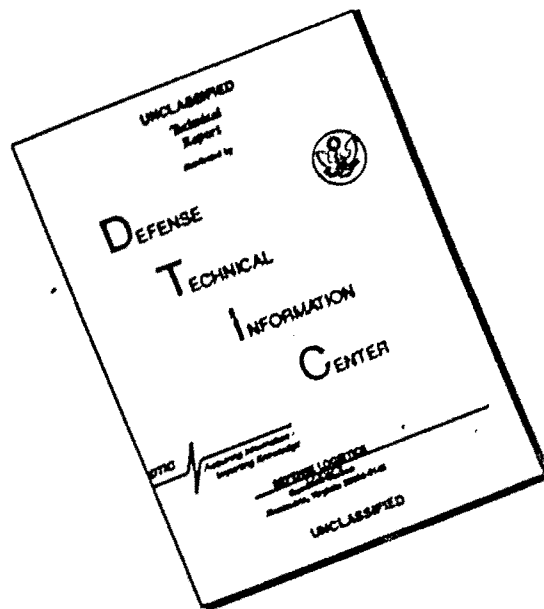
HEADQUARTERS FIELD COMMAND  
DEFENSE ATOMIC SUPPORT AGENCY  
SANDIA BASE ALBUQUERQUE NEW MEXICO



# ARCHIVE COPY

DDC  
RECEIVED  
OCT 29 1964  
DISPATCH  
TISA F

# DISCLAIMER NOTICE



THIS DOCUMENT IS BEST QUALITY AVAILABLE. THE COPY FURNISHED TO DTIC CONTAINED A SIGNIFICANT NUMBER OF PAGES WHICH DO NOT REPRODUCE LEGIBLY.

## NOTICE

This report is published in the interest of providing information which may prove of value to the reader in his study of effects data derived principally from nuclear weapons tests.

This document is based on information available at the time of preparation which may have subsequently been expanded and re-evaluated. Also, in preparing this report for publication, some classified material may have been removed. Users are cautioned to avoid interpretations and conclusions based on unknown or incomplete data.

PRINTED IN USA

Price \$2.25. Available from the Office of  
Technical Services, Department of Commerce,  
Washington 25, D. C.

**AD 607642**

WT-1528

**OPERATION PLUMBBOB**

**AD**

Project 26.4a

**4. SURFACE MOTION FROM AN UNDERGROUND DETONATION**

**L. M. Swift, Project Officer  
D. C. Sachs**

**Stanford Research Institute  
Menlo Park, California**

**April 1, 1959**

## ABSTRACT

Surface and near-surface acceleration and strain were measured on a deep underground nuclear burst (Rainier Shot; 900 feet; 1.7 kt) to permit extrapolation of results to nuclear detonations of other yields under different test or employment conditions. Results indicate that a large earth cap, probably including more than one chunk, separated from the mesa over the charge and subsequently fell back into place. The only significant vertical displacement occurred at or near ground zero and reached a maximum of approximately 0.9 feet. Both acceleration and horizontal surface strain measurements suggest that the principal disturbance on the mesa surface was confined to a small region around ground zero; however, the measurements on the slope indicate significant earth motion.

Velocity data (integrated accelerations) indicate that the layering characteristics of the medium exert a great influence upon the severity of the ground motion.

The displacement-time (double-integrated accelerations) data at surface zero agrees well with photographic data. In general, the peak displacements indicate that the cap rock moved up and away from surface zero, whereas the permanent displacements on the mesa show that the final positions of the stations are downward and inward toward surface zero, relative to pre-shot position.

From the preshot seismic survey and average velocities computed from the arrival time data, it is concluded that the medium of the Rainier mesa is many-layered with seismic velocities that are widely different. A reasonable profile is 5000 ft/sec from the surface to 200 feet, 10,000 ft/sec to 300 feet, and 6600 ft/sec to 1000 foot depth.

Although predicted strains were higher than those observed, horizontal surface strain results support the conclusion that the principal disturbance on the mesa was confined to a relatively small radius (less than 500 feet) around surface zero. Peak strains measured on the slope are significantly larger than expected at comparable ranges on the mesa.

## FOREWORD

The authors wish to acknowledge the excellent cooperation and guidance of Dr. R. G. Preston, Director, Program 26, and Mr. D. T. Schueler, Jr., of his staff. The effective assistance of Mr. J. M. Polatty of Waterways Experiment Station in design and execution of instrument grouting methods is also gratefully acknowledged.

The planning and execution of Project 26.4a were under the direction of Mr. L. M. Swift with Mr. W. Wells serving as field supervisor and Mr. L. H. Inman as field party chief. Other members of the field party included V. E. Krakow, C. M. Westbrook, R. V. Ohler, H. C. Wuner, and R. E. Amiller. Dr. D. C. Sachs wrote the report, while Dr. J. L. Brenner, Miss Barbara Ames, Miss Sherry Ward, Mrs. Barbara Wells, Mrs. Betty Hearn, and Miss Phyllis Flanders assisted in the data analysis and technical preparation of this report.

# CONTENTS

	<u>Page No.</u>
ABSTRACT . . . . .	2
FOREWORD . . . . .	3
CHAPTER 1 INTRODUCTION . . . . .	6
1.1 Objectives . . . . .	6
1.2 Background . . . . .	6
CHAPTER 2 EXPERIMENT PLAN . . . . .	8
2.1 Acceleration and Strain Measurements . . . . .	8
2.2 Predictions . . . . .	11
2.2.1 HE Equivalence . . . . .	11
2.2.2 Scaling Laws . . . . .	12
2.2.3 Acceleration . . . . .	12
2.2.4 Strain . . . . .	15
CHAPTER 3 INSTRUMENTATION . . . . .	18
3.1 Recording System . . . . .	18
3.2 End Instruments . . . . .	20
3.2.1 Accelerometers . . . . .	20
3.2.2 Strain Gages . . . . .	22
3.3 Instrument Response . . . . .	22
3.4 Timing Signals . . . . .	22
3.5 Power Supply . . . . .	23
3.6 Gage Coding . . . . .	23
CHAPTER 4 OPERATIONS . . . . .	24
CHAPTER 5 RESULTS . . . . .	25
5.1 Instrument Performance . . . . .	25
5.2 Data Reduction . . . . .	25
5.2.1 General . . . . .	25
5.2.2 Integration Procedures . . . . .	25
5.3 Gage Records and Tables of Results . . . . .	27
5.3.1 Acceleration . . . . .	27
5.3.2 Velocity . . . . .	27
5.3.3 Displacement . . . . .	28
5.3.4 Strain . . . . .	28
CHAPTER 6 DISCUSSION . . . . .	46
6.1 Earth Acceleration . . . . .	46
6.2 Earth Particle Velocity and Displacement . . . . .	56
6.2.1 Particle Velocity . . . . .	56
6.2.2 Particle Displacement . . . . .	60
6.3 Seismic Velocities . . . . .	64
6.4 Earth Strain . . . . .	68
6.5 Applicability of Project 26.4a Instrumentation . . . . .	73
6.5.1 Limitations of Experiment Plan . . . . .	73
6.5.2 Limitations of Instrumentation . . . . .	73
6.5.3 Suggested Improvements . . . . .	73
CHAPTER 7 CONCLUSIONS . . . . .	75
7.1 Instrumentation Performance . . . . .	75
7.2 Acceleration . . . . .	75
7.3 Velocity . . . . .	76
7.4 Displacement . . . . .	76
7.5 Seismic Velocities . . . . .	76
7.6 Strain . . . . .	77

CONTENTS (cont.)

	<u>Page No.</u>
CHAPTER 8 RECOMMENDATIONS . . . . .	78
APPENDIX A THE MEDIUM OF RAINIER SHOT . . . . .	79
APPENDIX B A NOTE ON PREDICTIONS FOR GAGE RANGE SETTING . . . . .	80
REFERENCES . . . . .	82
<b>TABLES</b>	
2.1 Gage Layout . . . . .	10
2.2 50-Ton Shot--Observed Peak Accelerations . . . . .	13
5.1 through 5.4 Acceleration, Velocity, Displacement and Strain, Rainier. . . . .	29-30
6.1 Permanent Displacement at SRI Gage Stations, Rainier .	64
6.2 Interval Velocities from USGS Data . . . . .	65
6.3 Seismic Velocities, Rainier . . . . .	67
6.4 Computed Vertical Strain in Deep Hole, Rainier . . . .	72
<b>FIGURES</b>	
2.1 Station layout . . . . .	9
2.2 Maximum acceleration vs distance . . . . .	14
2.3 Displacement and strain due to a buried pressure center	17
3.1 Recording station on the mesa surface . . . . .	19
3.2 Mesa surface: ground zero and vicinity . . . . .	19
3.3 and 3.4 Accelerometers on surface and slope of mesa. .	21
3.5 Typical strain gage installation . . . . .	23
5.1 Vertical acceleration, deep hole . . . . .	31
5.2 through 5.5 Vertical and horizontal acceleration . . . .	32-35
5.6 Vertical velocity, deep hole . . . . .	36
5.7 through 5.9 Vertical and horizontal velocity . . . . .	37-39
5.10 Vertical displacement, deep hole . . . . .	40
5.11 through 5.13 Vertical and horizontal displacement . . .	41-43
5.14 Horizontal and transverse strain. . . . .	44
5.15 Horizontal strain (surface and slope). . . . .	45
6.1 First peak vertical acceleration, deep hole . . . . .	46
6.2 Diagram of the effect of wave length on tension failure .	50
6.3 First peak horizontal and vertical acceleration . . . .	52
6.4 First peak horizontal and vertical acceleration . . . .	55
6.5 Earth velocity vs time, deep hole . . . . .	57
6.6 First peak vertical velocity, deep hole . . . . .	57
6.7 and 6.8 First peak horizontal and vertical velocity . . .	59
6.9 Earth displacement vs time, deep hole . . . . .	61
6.10 Comparison of GZ displacement (EG&G) with SRI data .	61
6.11 Vertical displacement contours at various times. . . .	61
6.12 First peak vertical displacement, deep hole. . . . .	62
6.13 and 6.14 First peak horizontal and vertical displacement	63
6.15 Velocity vs depth, Rainier and USGS seismic survey. .	66
6.16 Velocity vs slant range, Rainier . . . . .	66
6.17 Arrival time vs ground range . . . . .	69
6.18 Schematic of seismic rays from chamber . . . . .	69
6.19 Earth strain, Rainier. . . . .	71
6.20 Residual strain, Rainier Tunnel . . . . .	71

## CHAPTER 1

### INTRODUCTION

#### OBJECTIVES AND BACKGROUND

##### 1.1 OBJECTIVES

Program 26, associated with Shot Rainier (a deep underground detonation) at the Nevada Test Site, had as its general objective the development of sufficient data on earth motion (i.e., acceleration, strain, and displacement in the medium and on the surface and seismic disturbances on the surface) to permit extrapolation of the test results to nuclear detonations of other yields and under different test or employment conditions.

Specifically, the objective of Project 26.4a was to obtain data on the surface and near-surface earth motions produced by Shot Rainier, a 1.7-kt charge detonated approximately 900 feet below the ground surface.

##### 1.2 BACKGROUND

Rainier shot was designed to examine the feasibility of using underground shots for diagnostic testing of nuclear devices. The location chosen for Rainier was in Area 12 under the mesa forming the northwestern boundary of Yucca Flat. The material of the mesa was volcanic tuff, with a specific gravity of 1.6 to 1.9, overlaid by a cap of rhyolite (welded tuff) from 200 to 300 feet thick. (Reference 1 presents a more detailed description of the geology of the mesa; see also Appendix A of this report.)

The chief criterion for the proposed use of underground detonations is that the shot be "contained," that is, that it produce no appreciable off-site fallout. Unfortunately, very little applicable experimental data exist with which to determine the depth required for containment of a 1.7-kt charge in the material selected. Not only is there a dearth of data, but scaling of predictions over a wide range of yields leaves much to be desired, as is evident in a study of crater formation from shallow shots (Reference 2).

A great amount of information is available on the containment of relatively small high-explosives detonations in common soils and in rock formations; but the former is not applicable to the medium of Area 12, and the

latter is questionable because of the effects of "tamping" with other than original materials. Little pertinent data are to be had from the several large high-explosives shots conducted by the Corps of Engineers at moderate scaled depths in limestone, granite, and sandstone during their Underground Explosions Tests (1951) since none of these was deep enough to be completely contained (Reference 3).

In Nevada, only two previous underground nuclear shots were detonated: Jangle U and Teapot Ess (Shot 7), each with a yield of 1.2 kt and with charge burial depths of 17 and 67 feet, respectively (References 4 and 5). They were shot in the loosely-cemented conglomerate floor of Yucca Flat, not in the mesa tuff. Both shots produced large craters but not as large as had been generally predicted.

In view of the sparse background information on the characteristics of deep underground detonations in rock, it was decided to detonate two high-explosives shots (10 and 50 tons) in a tuff formation a few miles from Rainier site to aid the predictions for the Rainier shot. These shots were at lesser scaled depths than Rainier, and both may be considered to have been contained although pronounced surface effects were observed and the 10-ton shot vented through the access tunnel opening (Reference 6).

## CHAPTER 2

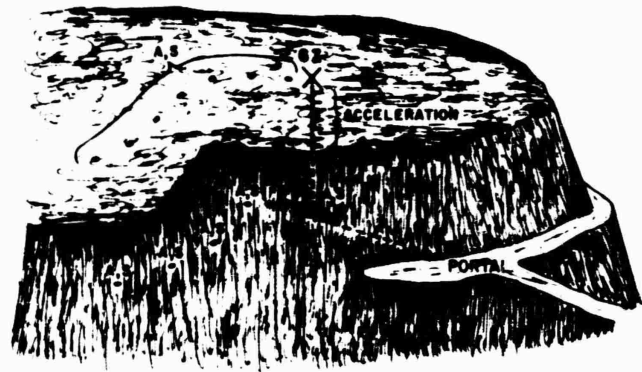
### EXPERIMENTAL PLAN

#### 2.1 ACCELERATION AND STRAIN MEASUREMENTS

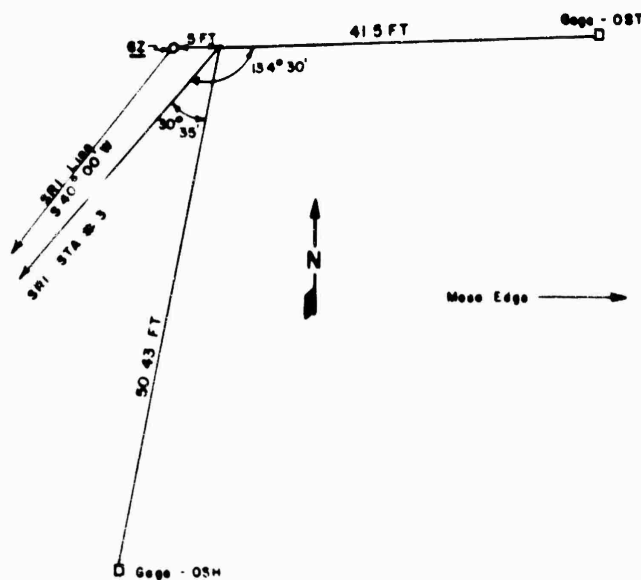
Station layout is shown in Figure 2.1 and Table 2.1. For an idealized view of the experiment plan, see sketch A. (Locations of acceleration and strain measurements are designated by A, S.)

Vertical acceleration was measured at 0, 100, 180, 250, and 320 feet below the mesa surface in a 350-foot hole over ground zero and at several ground ranges on the mesa surface and slope. Horizontal acceleration in the radial plane was measured at several surface ground ranges and at all but Station 10, that opposite ground zero, on the mesa slope.

Transverse strain was measured on the surface only at approximately 650 and 900 feet from ground zero. Horizontal radial strain was measured at approximately 0, 650, 900, and 1900 feet on the surface and at



Sketch A



Sketch B

approximately 0 and 400 feet on the slope. (Although the nomenclature for gages on this project indicates that one of the two strain gages at ground zero on the mesa surface is measuring transverse strain, in reality it is measuring horizontal strain since its reference point is the same as that for the horizontal strain gage and is located over ground zero, see sketch B at left.)

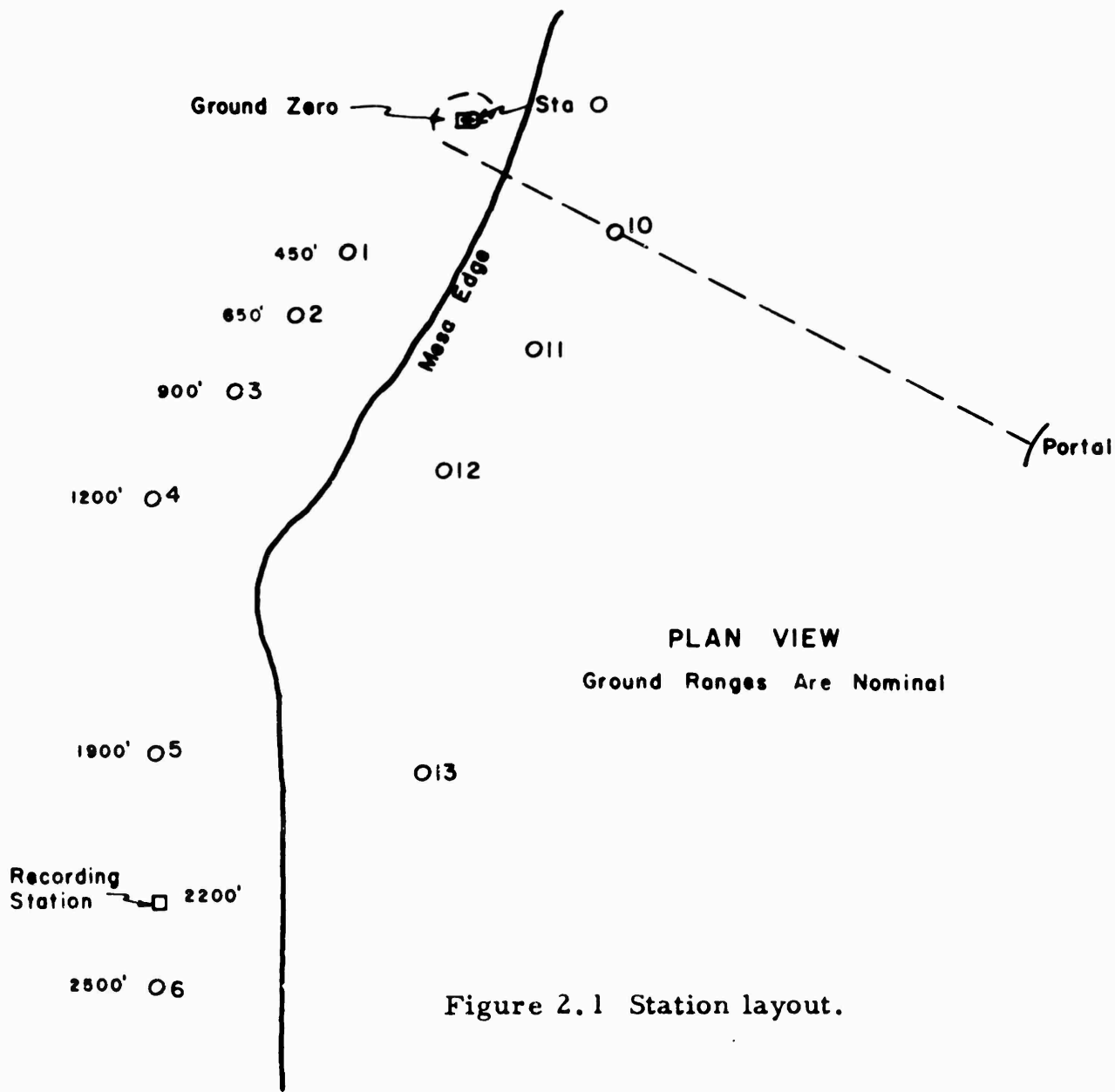
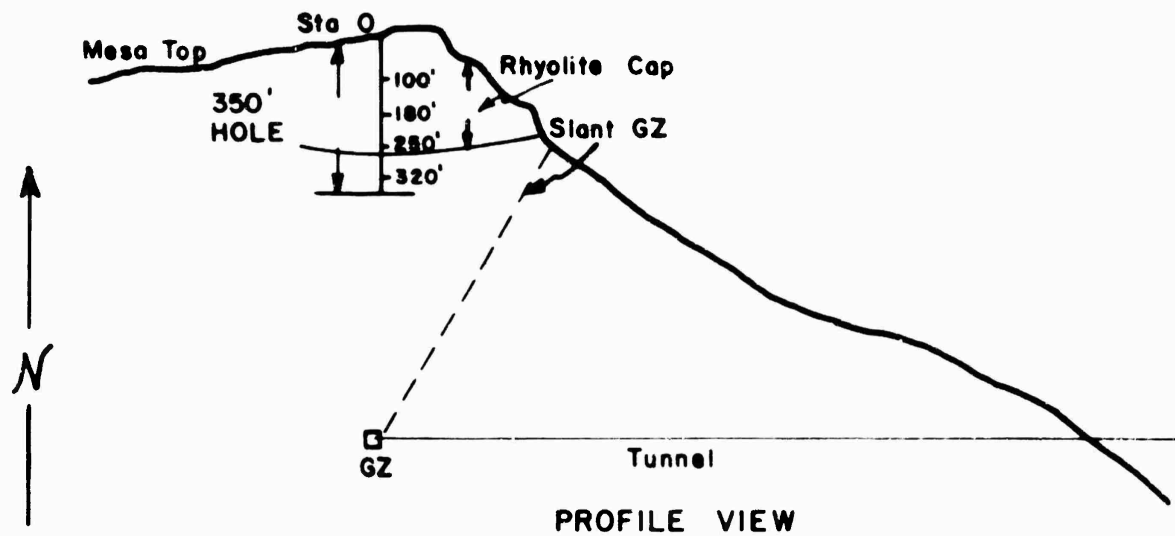


Figure 2.1 Station layout.

TABLE 2.1 GAGE LAYOUT

Nominal ground range, ft	Station No. and Gage code	Gage rating	Predicted peak <sup>a</sup>	Galvanometer, type Std -A	
0	OAP 0	5 g	1.5-3.0 g	3-3	
	Deep hole {	OAP 100 ft	5 g	2.0 g	3-2
		OAP 180 ft	5 g	3.0 g	3-2
		OAP 250 ft	10 g	5.0 g	3-2
		OAP 320 ft	10 g	6.6 g	3-2
		OSH	50.43-ft span	+5 ppk	3-3
	OST	41.5-ft span	+5 ppk	3-3	
450	1AP	5 g	1.1 g	3-2	
	1AH	1 g	0.3 g	3-3	
650	2AP	1 g	0.9 g	3-3	
	2AH	1 g	0.3 g	3-3	
	2SH	51.1-ft span	+1.3 ppk	3-3	
	2ST	54.6-ft span	+4.0 ppk	3-3	
900	3AP	1 g	0.8 g	3-3	
	3AH	1 g	0.3 g	3-2	
	3SH	62.3-ft span	-1.0 ppk	3-3	
	3ST	47.68-ft span	+1.8 ppk	3-3	
1250	4AP	1 g	0.6 g	3-3	
	4AH	1 g	0.3 g	3-3	
	4SH	100.25-ft span	-0.8 ppk	3-3	
1900 (1795) <sup>b</sup>	5AP	1 g	0.4 g	3-3	
	5AH	1 g	0.25 g	3-3	
	5SH	92.9-ft span	-0.6 ppk	3-3	
2500 (2340) <sup>b</sup>	6AP	1 g	0.35 g	3-3	
	6AH	1 g	0.25 g	3-3	
0	10AP	5 g	2.0 g	3-3	
	10SH	66.3-ft span	+8.0 ppk	3-3	
400 (+)	11AP	5 g	1.2 g	3-3	
	11AH	1 g	0.5 g	3-3	
	11SH	38.25-ft span	+2.5 ppk	3-3	
800 (+)	12AP	1 g	0.7 <sup>c</sup> g	3-3	
	12AH	1 g	0.4 g	3-3	
1500 (+)	13AP	1 g	0.5 g	3-3	
	13AH	1 g	0.3 g	3-3	

<sup>a</sup>Predicted peaks for acceleration are measured in multiples of force of gravity, g, and for strain in parts per thousand, vpk.

<sup>b</sup>Straight line distance from ground zero. (Stations 0-6 on mesa-range from mesa ground zero; stations 10-13 on slope-range approximately from slant ground zero.)

As shown in Figure 2.1, Stations 0 through 6 were on the mesa surface, Stations 10 through 13 on the slope. The deep hole (Sta 0) was drilled as close to ground zero as was practical, and the remaining mesa stations were laid out in a southerly direction from ground zero. The latter were placed at least 300 feet from the edge of the mesa to avoid any disturbances caused by jointing or planes of weakness in the rhyolite cap. Stations 10 through 13 were located at four positions on the face of the slope where the granular tuff was exposed just below the rhyolite-tuff interface. [ Stations 3 and 4 were jointly occupied by U.S. Coast and Geodetic Survey (USC&GS) and Stanford Research Institute (SRI). ]

## 2.2 PREDICTIONS

To select gage ranges and attenuator settings, it is necessary to predict the magnitude of phenomena resulting from the detonation. These predictions, however, are approached with a somewhat different attitude from that of analyses which are intended to develop a prediction technique. The approach is highly empirical and is colored by intuition based on experience and judgment of the quality of available data. A conscious effort was made to avoid the general tendency to over-predict effects, which had historically marred the effectiveness of projects associated with nuclear explosions, particularly underground explosions.

Predictions used for range settings were based largely on direct scaling of phenomena measured on the U.S. Geological Survey (USGS) 50-ton shot (Reference 6) and on the Underground Explosion Tests (UET) in Utah Sandstone (Reference 3). These tests were conducted in media resembling reasonably well the medium of Rainier site; Jangle U and Teapot Ess (Shot 7) were in a medium differing from that of Rainier and can be considered only for guidance in selecting lower limits of range settings.

2.2.1 HE Equivalence. The yield of a nuclear explosion is customarily stated in terms of the equivalent weight of TNT which would produce the same total energy release. In an aboveground nuclear explosion, it is well established that the mechanical (blast) effects are less than and other effects (thermal radiation, for instance) are greater than those produced by the corresponding amount of TNT. The HE equivalence of an aboveground nuclear explosion for airblast is about 46 percent; that is, a 1-kt device will produce the same blast effects as 0.46 kt of TNT.

The HE equivalence of an underground nuclear explosion for underground phenomena is not as well established. This equivalence is affected by a number of factors: the air space around the device, the density, heat of melting, and heat of vaporization of the medium, the water content of the medium, and the mass-to-yield ratio of the device, especially for small yields. Scaling problems have prevented accurate definition of HE equivalence of the two previous underground nuclear bursts in terms of all observed dynamic phenomena. However, calculations based on dynamic phenomena and on crater radius and volume suggest an HE equivalence for underground explosions of from 25 to 40 percent.

To be conservative, an HE equivalence of 40 percent was chosen for direct predictions for this project. This corresponds to an assumed HE yield of 0.68 kt, or  $1.36 \times 10^6$  lb of TNT.

2.2.2 Scaling Laws. For close-in phenomena, it is assumed that "cube-root" scaling holds; i. e., that observed phenomena at equivalent scaled ranges ( $R/W^{1/3}$ ) may be scaled appropriately to any size shot in the same or a similar medium. At the same scaled ranges peak strain (or particle velocity) is equal for any yield. Since the time factors change directly as  $W^{1/3}$ , scaled peak accelerations will vary inversely, and displacements directly, as  $W^{1/3}$ .

Direct scaling can be expected to apply only when all factors of geometry are scaled. At considerable distances from ground zero, and near the surface, reflections and refractions of energy may affect the phenomena markedly; in addition, it is important to consider differences in scaled charge depth and rock formation thickness in scaling from one shot to another.

2.2.3 Acceleration. In Reference 3 measured peak radial accelerations are presented from a number of 320-lb and three 40,000-lb HE shots in Utah Sandstone (UET). The latter were at a charge depth of only 12.5 feet ( $0.365 W^{1/3}$ ). The 320-lb charges were at depths ranging from 2.5 ( $0.365 W^{1/3}$ ) to 25 feet ( $3.65 W^{1/3}$ ). Since the 900-ft charge depth of Rainier represents a depth of about  $8 W^{1/3}$  for 0.68 kt (using 40 percent HE energy equivalence), the data from the deepest of these shots were considered the most pertinent, and the best-fit straight line through these data is shown in Figure 2.2, scaled to Rainier (0.68 kt HE equivalent). Note that the coordinates of the plot are acceleration and distance, rather

than ground range.

The USGS 50-ton shot was shot at a depth of 180 feet, a scaled depth of slightly under  $4 W^{1/3}$ , but in a medium closely resembling that of the Rainier site. The peak accelerations observed on the surface at several ranges are shown in Table 2.2, as are these values scaled to the Rainier shot. When these points are plotted on Figure 2.2, it is seen that all but one fall markedly below the scaled UET curve.

TABLE 2.2 50-TON SHOT-OBSERVED PEAK ACCELERATIONS

Sta	Slant range	A <sub>max</sub>	Scaled <sup>a</sup> slant range	Scaled <sup>a</sup> A <sub>max</sub>
	ft	g	ft	g
G0	180			
G0	180	62	405	27.0
B1	223	1	500	0.45
B4	250	1.75	560	0.78
B6	205	8.5	460	3.8

<sup>a</sup>To Rainier, 680 tons, scale factor 2.24.

For reference, the scaled acceleration-vs-distance curve for Teapot Ess (Shot 7) is also shown on Figure 2.2; this curve was obtained by direct scaling from 1.2 kt to 1.7 kt. The very low values on this curve represent an absolute lower limit since the shot was not contained and the medium for this shot was the unconsolidated sand and gravel of Yucca Flat. The change in slope of this curve, however, is typical of data from real explosions which include the effects of the surface and of reflections and refractions from deeper layers. The slope of the curve tends to change from about -4 at short radii to -2 or less at greater radii.

For range setting of channels measuring vertical acceleration, a prediction curve was drawn slightly below the scaled UET line at distances out to 1000 feet, then curving to a slope of about -2 at 3000 feet. On the basis of previous data, horizontal radial accelerations were predicted to be less than vertical, about half at close ranges, rising to about 75 percent at remote ranges.

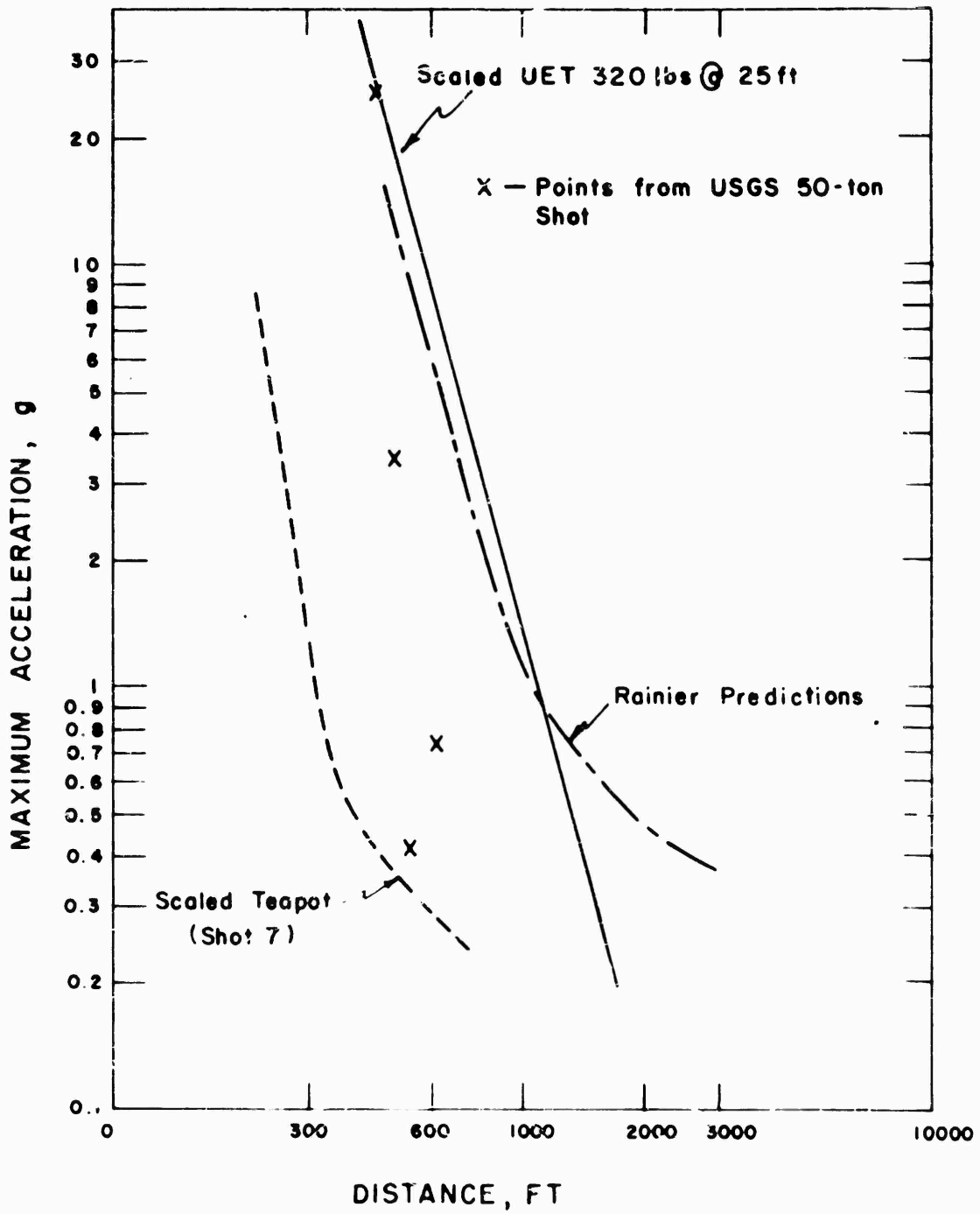


Figure 2.2 Maximum acceleration vs distance.

It should be noted also that although the magnitude of particle velocity in the medium ( $V$ ) is proportional to stress ( $S$ ), the direction of  $V$  is the direction of travel of the stress wave. Now, the acceleration is proportional to the stress space gradient,  $ds/dy$ , and equal to  $dv/dt$ . It is well known that a plane compressive (positive) stress wave upon reflection at a free surface becomes a plane tension (negative) wave in the same direction. Thus, as a consequence of the above relations, a downward-travelling negative stress pulse will cause velocity and acceleration in the same direction as an upward-travelling positive stress pulse. Finally, if ground motion is observed at a depth  $y$  between the surface and a source at a greater depth, one would also expect to observe at depth  $y$  the influence of the negative stress from the surface reflection.

2.2.4 Strain. The interest of this project in strain was limited to surface strain, as opposed to that in the interior of the medium. As yet, there appears to be no reliable method of tying the two together, except for a reasonable belief that surface strain is greater than that which would be present in the infinite medium if the surface were not present. Without detailing the data, it may be shown that scaling of strain data from the UET shots would predict compressive radial strains of the order of 8 to 20 parts per million at a 900-foot radius from shot Rainier in the semi-infinite medium. This may be taken as a lower limit when surface strain is considered.

The most profitable approach to the prediction of surface strain was considered to be its derivation from predicted displacement. Preliminary reduction of photographic data from the USGS 50-ton shot was reported to show a maximum upward displacement above ground zero of approximately 15 feet. This shot was at a scaled depth of about  $4W^{1/3}$ . Had it been at twice this depth (to correspond to Rainier), this displacement would have been less by a factor of about 8, or 2 feet, assuming slope of -3 of the curve of displacement-vs-slant range. Scaling this assumed displacement of 0.72-kt HE equivalent for Rainier produces a predicted maximum vertical displacement of slightly under 5 feet.

The larger an explosion, the longer the time scale of many of its major phenomena. Duration of the positive phase of the pressure pulse is greater for larger explosions, and as a consequence of this, the duration of the positive particle velocity, the duration of the positive displacement phase, and the time to return to steady state are all greater. For this reason, the transient

stress and displacement have time to adjust themselves more nearly to the values they would have in a stationary problem.

Assuming the medium to behave elastically, the equation of motion, and also the pressure at the shot chamber, are functions of time. There are additional conditions which say that the surface is free from stress, that there is a superimposed gravitational stress field, and that the pressure against the walls of the shot chamber is building up with time. If, at the time of the maximum displacement, the pressure against the walls of the shot chamber is constant, is equal to its maximum value, and  $d^2 \bar{u}/dt^2$  is zero ( $\bar{u}$  is the displacement vector), the problem then becomes one of finding the equilibrium (static) position of a large elastic solid under the influence of a buried pressure center. The solution reveals that the surface manifestation of the disturbance will be a pimple directly above the pressure center. In Appendix B, the problem and the analytic solution are reproduced from Reference 7.

While the assumption of elasticity is far from accurate, it is believed to give useful results in a real medium. Figure 2.3 shows the calculated variation with radial distance from zero of some of the pertinent parameters, normalized against  $W_0$  (maximum vertical displacement) and  $S_0$  (maximum infinitesimal strain at ground zero). In this figure, it is seen that while the vertical displacement and transverse strain decrease with ground range but never reverse, the radial displacement reaches a peak and the radial strain crosses zero at a ground range of  $0.707 h$ , where  $h$  is the depth of the charge below the surface. At ground ranges less than this value, the radial strain is tensile; at greater ground ranges, it is compressive.

In the regions where tensile strains were predicted, particularly, it seemed highly probable that the behavior would be inelastic, because of the jointed nature of the surface and near-surface medium. Such joints would not support tensile stress. Moreover, the infinitesimal strains are not expected to be the same for a dynamic problem as for a static one. However, long-span strains should be alike for both the static and the dynamic problems provided the span is sufficiently great. Without arguing the quantitative meaning of "sufficiently great," for prediction purposes it was felt that the general shape of the rise could be predicted well enough from elastic theory and that average strain predictions would be valid. The span (approximately 50 feet) of the strain gage was considered to be long, and the curves

of Figure 2.3 were used for range setting of the strain gages installed on the surface.

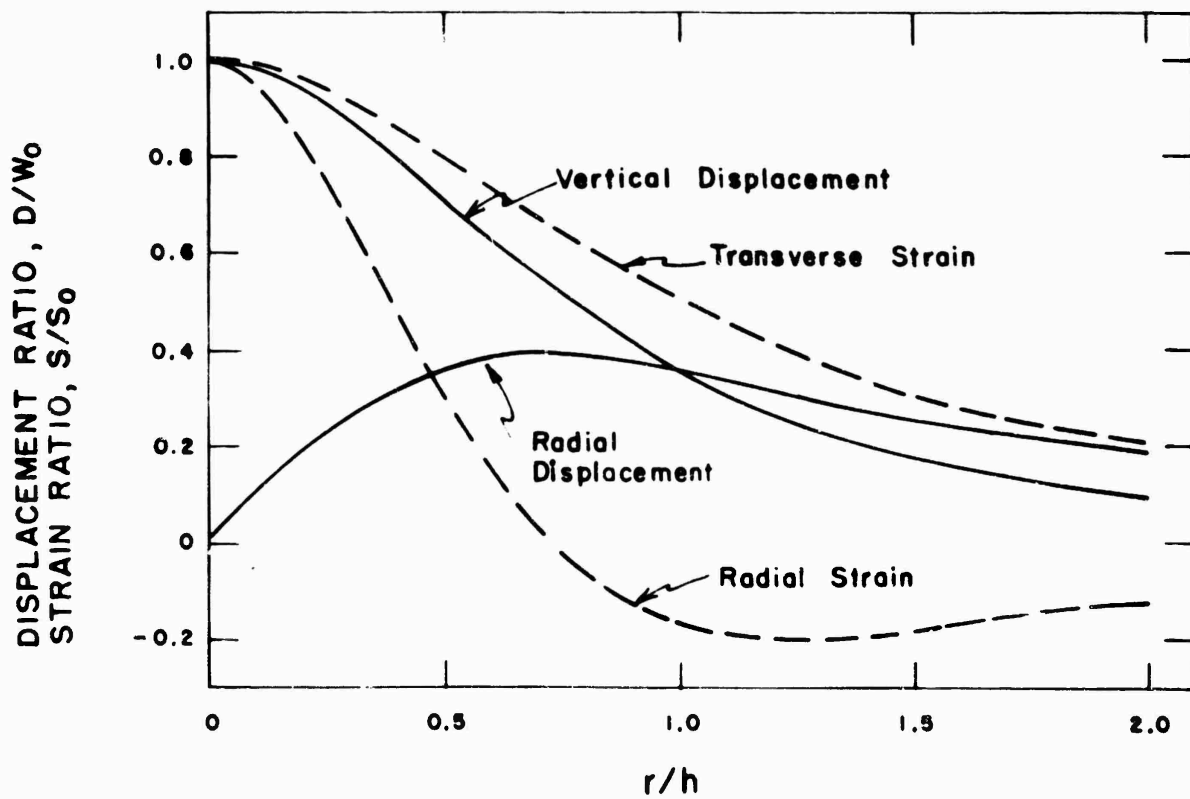


Figure 2.3 Displacement and strain due to a buried pressure center in a semi-infinite elastic medium ( $r$  = ground range, i.e., distance from ground zero;  $h$  = depth of burial).

## CHAPTER 3

### INSTRUMENTATION

All 34 channels of instrumentation were essentially the same electrically as those used on a number of previous projects (Reference 8).

#### 3.1 RECORDING SYSTEM

In general, the instrumentation consisted of Wiancko 3-kc oscillators supplying carrier power to end instruments (Wiancko variable-reluctance accelerometers) and to Wiancko demodulators. The demodulated signal was applied to and recorded on Miller Corporation oscillograph recorders. Each channel was dual-recorded to minimize loss of data from failure of a single recorder. On some of the dual channels, galvanometers having different sensitivities were used to provide a wide dynamic range of usable sensitivities.

A synthetic "calibrating signal" was automatically applied to each recording channel just prior to zero time. This signal was used to compare record deflections with those obtained by the same signal or "cal tap" at the time the channel was calibrated. A highly accurate timing signal of 100 and 1000 cps was also applied to all recorders simultaneously from a single source having a time accuracy of better than 10 parts per million. This gives the same time base to all records for time correlation of the separate events on all records.

All instrument recording gear was mounted in the SRI recording truck located on the mesa at approximately 2200 feet from ground zero (Figure 3.1). To prevent radiation damage to photographic records if Rainier shot were not contained, the oscillographs in the recording truck were protected by appropriate shielding. The truck body, camera cases, and paper magazines would afford a certain amount of shielding, about 0.5 cm of steel, 1.0 cm of aluminum, 5 feet of air, and 2 cm of paper. Thus, the inherent shielding in the truck would have an attenuation factor of about 0.5 for 0.35-Mev gamma radiation.



Figure 3.1 Recording station on the mesa surface (recording truck under canopy).



Figure 3.2 Mesa surface: Ground zero and vicinity, looking south. A - SRI, Station C, deep hole (accelerometers); B - Mesa edge; C - Sandia installation; D - SRI surface gage line; E - Ground zero (behind pipe).

If the radiation were as much as 15 r (infinite exposure) this shielding would reduce the level to 7.5 r, and recovery at H + 5 hours (200 mr/hr) would cut this amount to 5.2 r, giving a shielding factor of over 2. To increase the shielding factor still more, the oscillographs were shielded with lead bricks and lead sheets. This was done by stacking 1-1/2-inch thick lead bricks at the rear of the oscillographs opposite the paper magazines and placing 1/2-inch thick lead sheets under the oscillographs and on a framework which covered the tops and the fronts of the oscillographs. This covering gave a shielding factor of 30 or more.

### 3.2 END INSTRUMENTS

3.2.1 Accelerometers. Standard Wiancko variable-reluctance accelerometers were used (Reference 9). The accelerometers in the deep hole at Station 0 (Figure 3.2) were installed in the following manner: A 1/4-inch wire cable, which had been prestretched, was weighted and lowered into the hole. At measured points on the cable, the appropriate accelerometer for that depth was attached, together with its signal cable. At three points, as the entire array was being lowered into the hole, one-inch plastic hoses were also attached to the cable. After the accelerometers were stopped at the designated depths, a special grout, specified by Waterways Experiment Station, was pumped down these hoses until the hole was filled. Those on the mesa surface were encased in canisters which carried two accelerometers mutually perpendicular to each other so that both vertical and horizontal accelerations could be measured. The canisters were grouted in holes drilled or dug in the rhyolite cap (Figure 3.3).

Accelerometers on the slope were mounted in perpendicular and radial positions by fastening them to wooden blocks which in turn were attached to the tuff by two bolts grouted into drilled holes (Figure 3.4). Accelerometers in the deep hole at ground zero were calibrated by use of a spin table with accelerations up to approximately 10 g. Accelerometers on the mesa and on the slope were calibrated in the earth's field by use of a turn-over cradle which gave equivalent accelerations to 2 g.

Accelerometers were calibrated in the field after they had been connected to their cables and associated recording equipment just prior to being grouted into the rock.



Figure 3.3 Accelerometer installed on surface of mesa.



Figure 3.4 Accelerometer installed on slope of mesa.

3.2.2 Strain Gages. The earth strain gages used on this project were an adaptation of the Ballistics Research Laboratory long-span displacement gages. They consisted essentially of a potentiometer whose shaft is arranged so that it can be rotated by a sheave wheel on the end of the shaft. A long length of piano wire was anchored at a distant point and was also attached to the sheave wheel. This wire was kept under tension by a coil spring so that any change in the relative position of the gage to the distant anchor results in a rotation of the potentiometer shaft thus indicating the change in the relative position of the two measured points.

Strain gages on the mesa surface and slope were mounted on a plywood board which in turn was anchored to the solid rhyolite by four bolts, which were also grouted into drilled holes (Figure 3.5). The eye bolts for attaching the wire at the other end were also grouted to the rhyolite. The strain gages were calibrated with 1- to 4-inch displacement blocks at the end of the wire span away from the gage and the appropriate deflection noted.

### 3.3 INSTRUMENT RESPONSE

The Wiancko accelerometer and its associated recording system is basically flat down to steady-state conditions due to its design as a carrier-demodulator system. No correction therefore is required for its low frequency response. The high frequency response is limited either by the characteristics of the galvanometers or by the dynamic characteristics of the transducers. The 300-cps galvanometers (nominal) had a natural frequency of 315 to 340-cps and were damped to have an overshoot of approximately 7-1/2 percent. This corresponds to a damping factor of approximately 0.65 critical and provides a nominal rise time of 1.3 milliseconds. The 200-cps galvanometers were also critically damped and had a correspondingly longer rise time of approximately 1.8 milliseconds.

The accelerometers varied in sensitivity from 1 g to 10 g and in general had low natural frequencies so that the limiting frequency response was generally that of the accelerometers.

### 3.4 TIMING SIGNALS

Instruments were energized by Edgerton, Germeshausen, and Grier (EG&G) timing signals that actuated lock-in relays controlled by a time-delay relay which allowed continued instrument operation for approximately two minutes after zero time, even though EG&G relays dropped out sooner.

### 3.5 POWER SUPPLY

During the shot, all instruments and recorders were supplied with power by banks of heavy-duty batteries. Converters were used to produce 115-volt alternating current for instruments requiring this power. Individual converters were used for each rectifier power supply to minimize possible gross failure due to converter failure. During calibration and testing before the shot, a 10-kw motor generator was used as a power source.

### 3.6 GAGE CODING

For identification of channels and recorded traces with their proper gages, a systematic coding was used. The first part of the gage code is the station number. Letters which indicate the type of measurement form the second part of the gage code. On this project the letters AP denote vertical or perpendicular acceleration; that is, vertical or perpendicular with reference to the natural terrain. The gages on the mesa surface and in the hole would be vertical while those on the slope would be perpendicular to the tuff out-crops but not necessarily perpendicular to the horizontal plane. AH denotes horizontal radial acceleration, ST denotes transverse strain, and SH denotes horizontal radial strain. The third part of the gage code, applicable only at Station 0 indicates the depth of the gage below the surface in feet. Typical gage code numbers would then be as follows: 3AP for Station 3, vertical acceleration; OAP180 for Station 0, vertical acceleration at a depth of 180 feet.

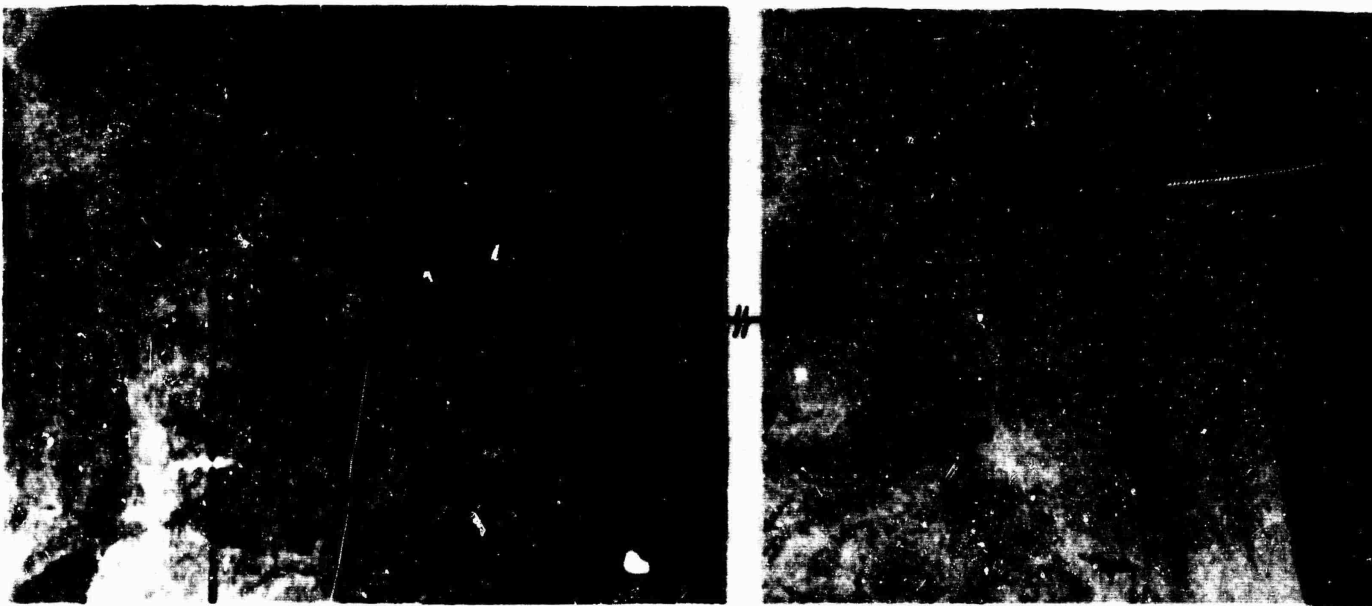


Figure 3.5 Typical strain gage installation (spans vary).

## CHAPTER 4

### OPERATIONS

The site of operations was examined on April 26, 1957, and at that time a location for the recording truck was chosen. The mesa was scouted, and the direction and approximate location of the line of accelerometer and strain gage stations was also chosen. The mesa slope was traversed, and four places were picked for installation of stations just below the rhyolite-tuff interface.

Field operations in preparation for this project were started on August 13. All the cables to surface stations on this project were laid on the ground only, protected by culverts where they crossed roads. By August 21 cables were laid, instruments connected, and calibration begun. Some time was lost because of fallout from Shots Galileo and Fizeau; however, all gages were in place and calibrated by September 17. Final timing runs were made on September 18, and the instruments were checked and made ready in the evening of September 18. The shot, which was originally scheduled for September 18, was delayed 24 hours and detonated at 1000 hours on September 19. The shot did not vent; and after a few hours, the road to the top of the mesa was opened, and recovery of the records was made that afternoon.

## CHAPTER 5

### RESULTS

#### 5.1 INSTRUMENTATION PERFORMANCE

All 34 instrument channels gave usable records, although 4 were incomplete due to cable breaks during the active portion of the record. The breaks occurred in the cables associated with the underground accelerometers; however, enough of each gage record was obtained to lead to definitive conclusions.

Since some of the predicted values for peak acceleration were low, some of the gage records exceeded the boundaries of the recording paper. Nevertheless, since each gage record was recorded twice, often with galvanometers of different sensitivities, it was possible in almost all cases to determine the magnitude of the peak acceleration at each station.

All accelerometers and strain gages on the mesa top were recovered and appeared to suffer no permanent damage. On the slope, Station 10 gages were lost due to a rock slide in that vicinity; one accelerometer was missing at Station 11, also probably the victim of falling rock; the gages at Stations 12 and 13 were recovered intact.

#### 5.2 DATA REDUCTION

5.2.1 General. After each record was identified on the oscillograms, it was "read" (inches deflection of record versus time) with an electro-mechanical reader, Benson-Lehner "Oscar" Model J. The reader output was fed into an IBM card punch, which produced the data cards. These deflection-versus-time data cards, along with appropriate calibration cards, were processed by an IBM Model 650 electronic computer. The final reduced data consisted of the parameter (e.g., acceleration) versus time listings corresponding to each gage record. These listings were then plotted to yield the data upon which this report is based.

5.2.2 Integration Procedures. The earth acceleration-versus-time data were integrated successively to obtain, first, the particle velocity

versus time, and second, the particle displacement versus time. Acceleration records were read at 1-millisecond intervals throughout the portion of maximum fluctuation. As the records smoothed out, this time interval was lengthened successively to 2, 5, and 10 milliseconds. Records were read to the time on the acceleration record at which little or no apparent motion was evident.

Undeniably, the ground motion from an underground explosion must cease at some time after the detonation. Most integrations indicate, in varying degree, the velocity at the end of the integration (of acceleration time) is non-zero. This result can be interpreted as an acceleration record "baseline shift," which is manifest during the recording or during the reading of the record. If it can be assumed that there are no frequency response problems, the source of the difficulty can be traced to the character of the acceleration-time waveform. Usually, the duration of the first acceleration peak is a small fraction of the total record length. Therefore, a small error, perhaps only one or two percent of the peak acceleration (i. e., corresponding to perhaps only one or two Oscar counts), will accumulate as time increases to produce a significant error in velocity at the end of the integration.

In work with small high-explosive charges, acceleration-time records are of short duration, and it is straightforward to determine the time beyond which there is no significant earth motion. However, for Rainier, this determination is complicated by the fact that refracted and reflected waves (of greatly reduced amplitude compared with the first arrivals) are detected long after the arrival of the first disturbance. It seems to be a misuse of time and money to read and integrate the acceleration records to excessively long times following arrival; for this reason, the Rainier acceleration records were read and integrated to a time at which acceleration amplitudes have diminished to very small values and the waves have periods of 0.2 second or longer.

Since there are really no definitive criteria for determining the time-of-zero earth velocity associated with an underground nuclear explosion, it was decided that no effort would be made to correct the velocity and displacement integrations for possible baseline shift. Therefore, the integrations are reported uncorrected, and they will be discussed on that basis.

### 5.3 GAGE RECORDS AND TABLES OF RESULTS

Figures 5.1 through 5.15 present the significant portion of the re-plotted gage records and integrations obtained on this project. The acceleration-time records are found in Figures 5.1 through 5.5; these figures include arrival time of the first disturbance at each station and the magnitudes of the principal maxima. The order of presentation is deep hole, surface level, and slope line, with the vertical (AP) preceding the horizontal (AH) record at each station. The earth velocities (integrated acceleration) are presented in Figures 5.6 through 5.9, and the displacements in Figures 5.10 through 5.13. The strain measurements are shown in Figures 5.14 and 5.15.

All the records are plotted to the same time scale; however, to obtain the best compromise between economy of space and faithful reproduction of the details of the records, it was necessary to replot some of the records to an ordinate scale increased by a factor of five (see Figures 5.2 and 5.5).

5.3.1 Acceleration. The underground acceleration measurements taken in the deep hole over the shot point are given in Figure 5.1, which includes all of the records influenced significantly by cable breakage. The records indicate that the cable broke earliest at the deepest station (320-feet deep) and latest at the shallowest underground station (100-feet deep). The vertical acceleration on the surface (mesa) and the slope are mainly characterized by a single peak of acceleration in the upward direction (away from the ground surface and detonation point) followed by a fairly constant, flat downward acceleration and a second sharp upward peak. On the other hand, horizontal acceleration waveforms exhibit a small outward peak acceleration followed by an interval of zero acceleration and then a sharp inward (or outward) peak. At the greater ranges, Stations 5, 6, and 13, the waveforms possess no definitive form; at these ranges the reflected and refracted waves predominate and tend to mask any systematic behavior. The basic acceleration data are listed in Table 5.1.

5.3.2 Velocity. Figure 5.6 presents the vertical velocity-time plots from the deep hole measurements. Even with the incomplete records, it is evident that the velocity at all depths rises to its maximum soon after wave arrival and decays somewhat more slowly to zero velocity before downward velocities are manifest. The vertical velocity-time records obtained on the mesa (Figures 5.7 and 5.8) are similar in form to those obtained in

the deep hole. The records appear to approach zero or very small velocities near 1.20 or 1.40 seconds, after which some of the plots deviate somewhat from the baseline (e.g., OAPA and 3AP). However, the horizontal velocities are characterized by a rather flat-topped response away from ground zero followed by a more prominent velocity toward zero; also, the horizontal component velocities deviate markedly from the baseline beyond about 1.40 seconds. Large deviations such as those shown on records 1AH, 2AH, and 3AHA are believed to be due to baseline errors, because reference to the corresponding acceleration-time records (Figures 5.1 and 5.2) reveals that one is dealing with very small magnitudes after about 0.8 second. In addition, the constant slope deviation from the baseline of the integrated (velocity) record, e.g., 1AH near 1.40 seconds, is characteristic of a baseline shift. Thus, integration beyond this point is not reliable. The velocity data are presented in Table 5.2.

5.3.3 Displacement. The results of the double integration of the acceleration records are presented in Figures 5.10 through 5.13. The vertical displacements measured in the deep hole (Figure 5.10) indicate that peak displacements were recorded at the surface and at 100-foot depth before the cables broke, but for the deeper depths, particularly 320 and 180 feet, the displacement-time curve is rising at the time of cable break. Also, as was pointed out for the velocity plots, the OAPA displacement is probably not reliable beyond 1.20 seconds. As expected, Figure 5.11 shows that the horizontal displacement-time records are more difficult to interpret than the vertical. The first peak of displacement is probably the only reliable data derived from the double integration procedure. Displacement data are presented in Table 5.3.

5.3.4 Strain. The earth strain-time records presented in Figures 5.14 and 5.15 show no characteristic form. The strains measured at ground zero (OSH and OST) are similar in form--but, as pointed out in Section 2.2.4, at ground zero these two measurements are equivalent. The same is not true at the other mesa stations; thus, it is expected that the horizontal strains (SH) will exhibit a different form from the transverse strains (ST). At stations other than at ground zero the horizontal strains indicate compressive strain followed by a tensile strain. However, no tensile strain is observed at Stations 4 and 5 (Figure 5.15). (Note: There is an enlarged strain scale used for the 4SHA and 5 SH plots.) On the slope, the principal strains are tensile. Table 5.4 summarized the strain data.

TABLE 5.1 PEAK ACCELERATION, RAINIER

Gage code	Ground range ft	Slant range ft	Type of measurement	Arrival time sec	Acceleration					
					First peak g	sec	Max. positive g	sec	Max. negative g	sec
----- Deep Hole -----										
OAPA	0	889.5	Vertical	0.144	5.78	0.184	5.78	0.184	1.09	0.288
OAP 100	0	799.5	"	.124	4.00	.148	4.00	.148	0.98	.348
OAP 180A	0	719.5	"	.109	1.46	.130	1.46	.130	CB <sup>a</sup>	.324
OAP 250A	0	649.5	"	.100	1.36	.120	1.36	.120	CB <sup>a</sup>	.324
OAP 320	0	579.5	"	.088	5.78	.106	5.78	.106	CB <sup>a</sup>	.204
----- Surface -----										
1AP	458.4	970.9	Vertical	0.157	3.20	0.185	5.92	0.407	0.90	0.233
1AH	"	"	Horizontal	.157	1.04	.189	2.23	.417	4.10 <sup>b</sup>	.407
2AP	654.8	1095	Vertical	.179	2.79	.209	8.16 <sup>b</sup>	.433	0.94	.327
2AH	"	"	Horizontal	.177	0.90	.203	5.04 <sup>b</sup>	.427	3.13 <sup>b</sup>	.433
3AP	901.7	1265	Vertical	.202	1.40	.226	1.40	.226	0.87	.316
3AHA	"	"	Horizontal	.202	0.60	.228	0.65	.698	.80	.476
4AP	1273	1553	Vertical	.245	.77	.281	1.78	.467	.65	.361
4AH	"	"	Horizontal	.245	.59	.305	0.59	.305	.57	.537
5AP	1732	1957	Vertical	.296	.61	.356	.84	.538	.63	.468
5AH	"	"	Horizontal	.296	.93	.358	1.62	.764	.99	.582
6AP	2339	2518	Vertical	.359	.35	.419	0.43	.601	.45	.461
6AH	"	"	Horizontal	.361	.33	.427	.45	.861	.33	.725
----- Slope -----										
10APA	480.9	797.1	Vertical	0.146	7.90	0.170	7.90	0.170	2.93	0.202
11APA	600.5	860.4	Vertical	.144	8.59 <sup>b</sup>	.169	9.67 <sup>b</sup>	.636	5.62 <sup>b</sup>	.488
11AHA	"	"	Horizontal	.146	2.91	.170	7.55 <sup>b</sup>	.634	7.71 <sup>b</sup>	.486
12APA	880.7	1084	Vertical	.173	1.52	.213	1.94	.407	0.90	.293
12AHA	"	"	Horizontal	.173	1.33	.215	1.33	.215	1.48 <sup>b</sup>	.443
13APA	1656	1774	Vertical	.274	0.39	.324	0.43	.492	0.83	.362
13AHA	"	"	Horizontal	.276	.48	.328	.76	.530	.38	.556

<sup>a</sup>CB - cable break.

<sup>b</sup>Peaks estimated, trace being off record.

TABLE 5.2 PEAK VELOCITY, RAINIER

Gage code	Ground range ft	Slant range ft	Type of measurement	Arrival time sec	Velocity			
					Max. positive ft/sec	sec	Max. negative ft/sec	sec
----- Deep Hole -----								
OAPA	0	889.5	Vertical	0.144	6.28	0.216	7.19	0.632
OAP 100	"	799.5	"	.124	5.13	.224	CB <sup>a</sup>	.468
OAP 180A	"	719.5	"	.109	1.73	.186	CB <sup>a</sup>	.324
OAP 250A	"	719.5	"	.100	1.20	.176	CB <sup>a</sup>	.324
OAP 320	"	579.5	"	.088	3.46	.128	CB <sup>a</sup>	.204
----- Surface -----								
1AP	458.4	970.9	Vertical	0.157	2.04	0.201	3.05	0.403
1AH	"	"	Horizontal	.157	0.62	.389	1.53	.695
2AP	645.8	1094	Vertical	.179	2.00	.225	2.81	.427
2AH	"	"	Horizontal	.177	1.21	.431	1.53	.635
3AP	901.7	1264	Vertical	.202	1.40	.264	1.44	.394
3AHA	"	"	Horizontal	.202	1.04	.440	1.35	.674
4AP	1273	1553	Vertical	.245	0.93	.309	1.22	.449
4AH	"	"	Horizontal	.245	.78	.337	1.22	.647
5AP	1732	1957	Vertical	.296	.77	.376	1.12	.518
5AH	"	"	Horizontal	.296	1.48	.400	1.89	.724
6AP	2339	2518	Vertical	.359	0.43	.443	0.56	.553
6AH	"	"	Horizontal	.361	.44	.455	.61	.785
----- Slope -----								
10APA	480.9	797.1	Vertical	0.146	5.75	0.194	3.32	0.792
11APA	600.5	860.4	Vertical	.144	4.58	.202	3.03	.626
11AHA	"	"	Horizontal	.146	1.93	.262	3.09	.520
12APA	880.7	1084	Vertical	.173	1.45	.225	1.30	.371
12AHA	"	"	Horizontal	.173	1.55	.245	2.34	.473
13APA	1656	1774	Vertical	.274	0.37	.334	0.63	.410
13AHA	"	"	Horizontal	.276	.47	.338	.19	.504

<sup>a</sup>CB - cable break.

TABLE 5.3 PEAK DISPLACEMENT, RAINIER

Gage code	Ground range ft	Slant range ft	Type of measurement	Arrival time sec	First peak ft	Second peak sec	Second peak ft	End of integration ft	End of integration sec	
- - - - - Deep Hole - - - - -										
OAPA	0	889.5	Vertical	0.144	0.882	0.416		-3.933	2.000	
OAP 100	"	799.5	"	.124	.830	.416	CB <sup>a</sup>	0.468	CB <sup>a</sup>	
OAP 180A	"	719.5	"	.109	.229	.324	CB <sup>a</sup>	.324	CB <sup>a</sup>	
OAP 250A	"	649.5	"	.100	.119	.268	CB <sup>a</sup>	.324	CB <sup>a</sup>	
OAP 320	"	579.5	"	.088	.311	.204	CB <sup>a</sup>	.204	CB <sup>a</sup>	
- - - - - Surface - - - - -										
1AP	458.4	970.9	Vertical	0.157	0.136	0.289	-0.070	0.553	-0.669	2.001
1AH			Horizontal	.157	.121	.431	-	-	2.235	2.001
2AP	654.8	1094	Vertical	.179	.156	.327	-.014	.520	-0.645	2.001
2AH			Horizontal	.177	.173	.489	-.139	.933	1.228	2.001
3AP	901.7	1246	Vertical	.202	.094	.326	-.039	1.000	-0.677	1.960
3AHA			Horizontal	.202	.189	.496	-.156	1.040	-1.201	1.960
4AP	1273	1553	Vertical	.245	.062	.373	-.015	0.485	0.101	1.361
4AH			Horizontal	.245	.146	.527	-.101	.929	.062	1.505
5AP	1732	1957	Vertical	.296	.047	.436	-.044	.586	.058	0.956
5AH			Horizontal	.296	.160	.578	-.289	1.192	-.160	1.504
6AP	2339	2518	Vertical	.359	.022	.489	-.031	0.853	.044	1.113
6AH			Horizontal	.361	.031	.685	-.039	.873	-.042	1.207
- - - - - Slope - - - - -										
10APA	480.9	797.1	Vertical	0.146	0.982	0.622	-	-	0.068	1.504
11APA	600.5	860.4	Vertical	.144	.499	.370	-0.267	1.136	-.021	1.504
11AHA			Horizontal	.146	.213	.488	-.082	0.634	.712	1.504
12APA	880.7	1084	Vertical	.173	.097	.301	.105	.937	-.238	1.505
12AHA			Horizontal	.173	.159	.375	-.240	.649	-.751	1.505
13APA	1655	1774	Vertical	.274	.013	.360	-.042	.560	-.139	1.504
13AHA			Horizontal	.276	.036	.470	-	-	.704	1.504

<sup>a</sup>CB - cable break.

TABLE 5.4 PEAK STRAIN, RAINIER

Gage code	Ground range ft	Slant range ft	Type of measurement	Arrival time sec	First peak ppk	Second peak sec	Second peak ppk	Residual strain ppk	Residual strain sec	
- - - - - Surface - - - - -										
OSH	0	889.5	Horizontal	0.198	3.461	0.580	-0.622	0.850	1.666	3.500
OST			Transverse	.164	-0.495	.192	4.510	.604	1.815	3.700
2SH	654.8	1094	Horizontal	.214	-.252	.340	0.497	1.140	0.361	3.500
2STA			Transverse	.362	.233	.610	-.244	0.990	-.157	3.700
3SH	901.7	1264	Horizontal	.368	-.061	.386	.189	1.490	.104	3.500
3ST			Transverse	.448	.621	.584	-.100	0.875	.204	3.700
4SHA	1273	1553	Horizontal	.296	-.059	.618	.012	.970		3.500
5SH	1732	1957	Horizontal	.337	-.099	.539	-	-	-.020	3.700
- - - - - Slope - - - - -										
10SHA	480.9	797.1	Horizontal	0.173	-1.416	0.501	3.050	0.791	-3.316 <sup>a</sup>	1.001
11SHA	600.5	860.4	Horizontal	.168	-0.314	.218	5.198	.628	0.198	3.700

<sup>a</sup>Cable break at 1.031.

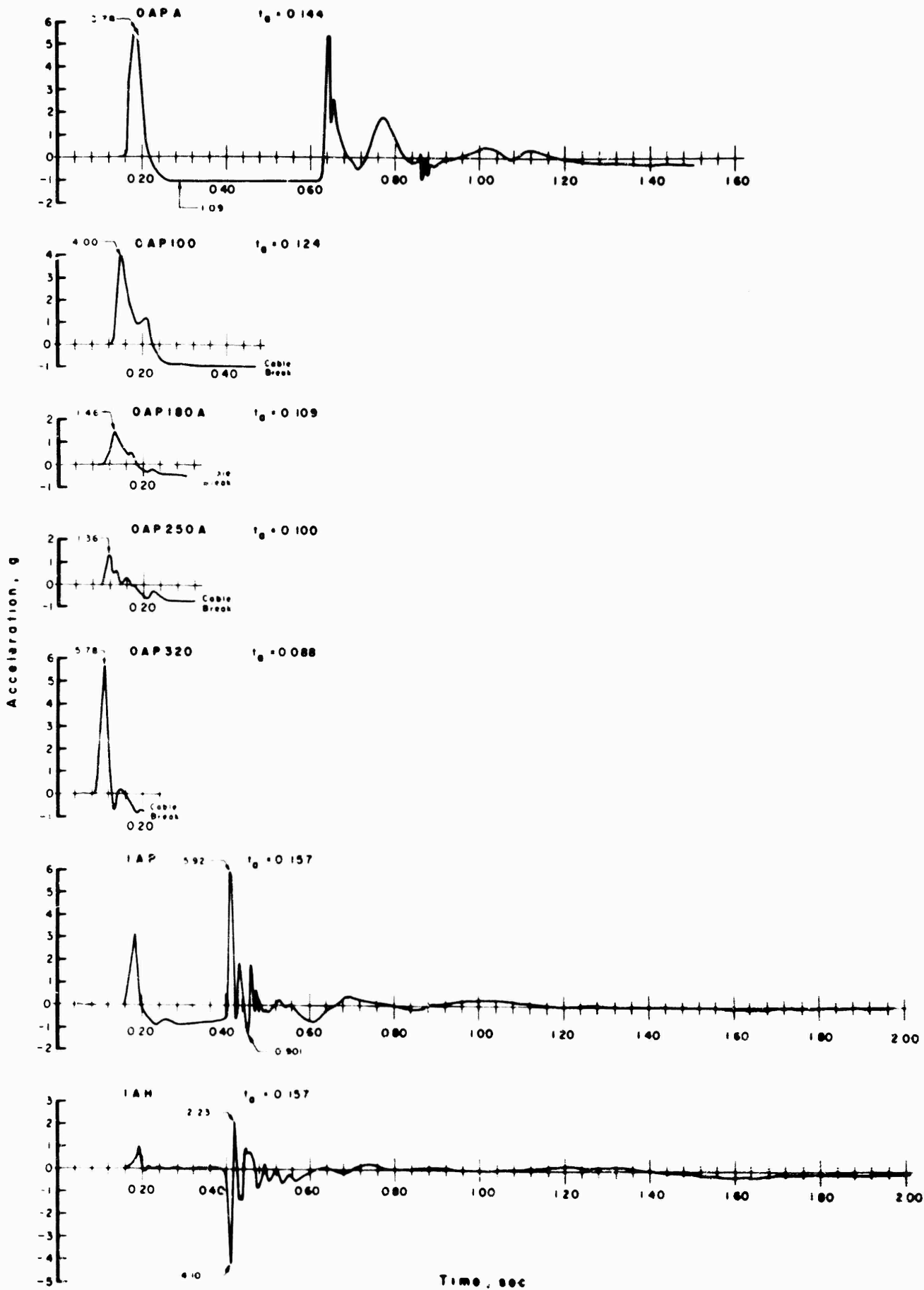


Figure 5.1 Vertical acceleration, deep hole; and vertical and horizontal acceleration, Station 1 (surface).

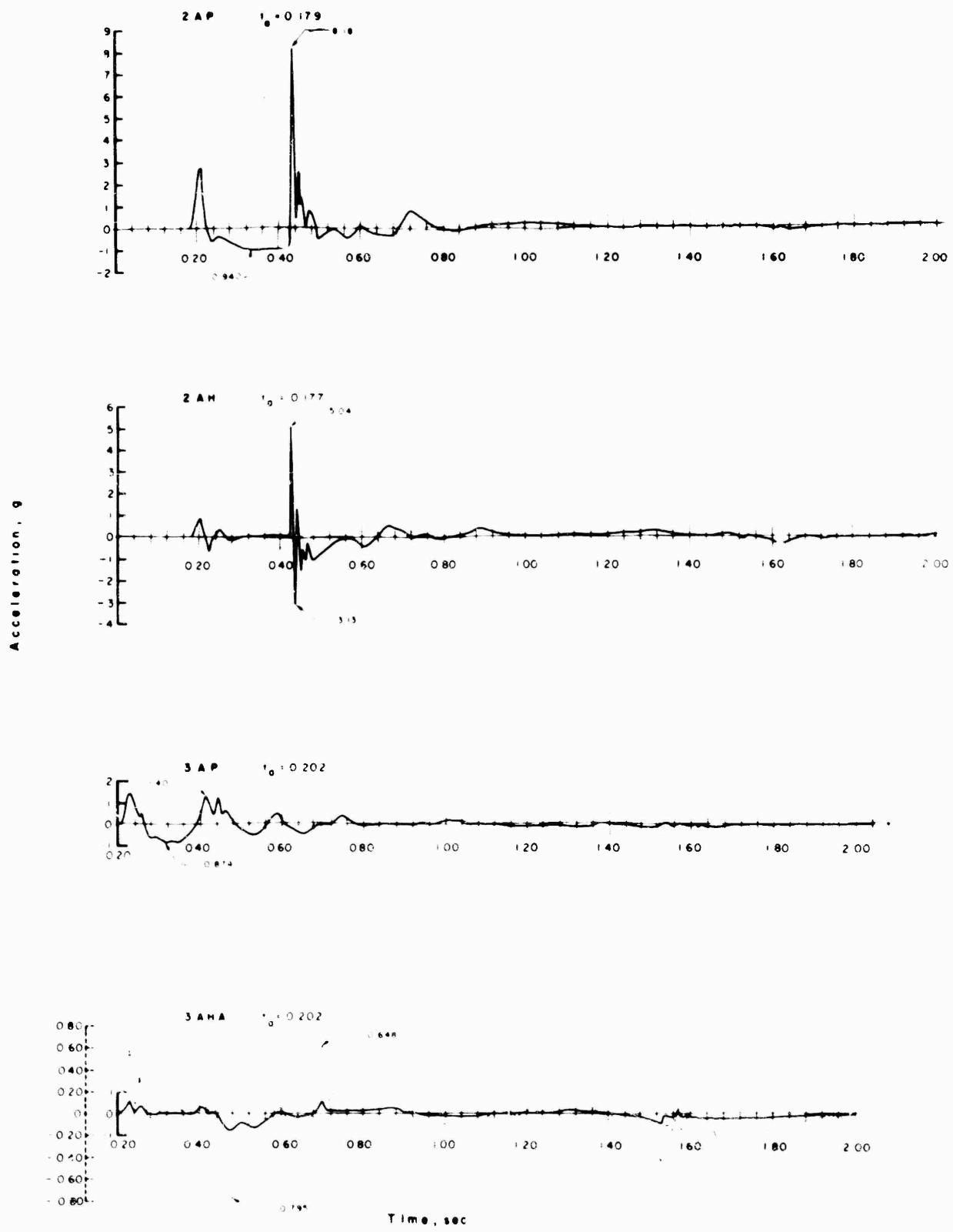


Figure 5.2 Vertical and horizontal acceleration, Stations 2 and 3 (surface). (Broken line shows replot with ordinate scale increased by a factor of five.)

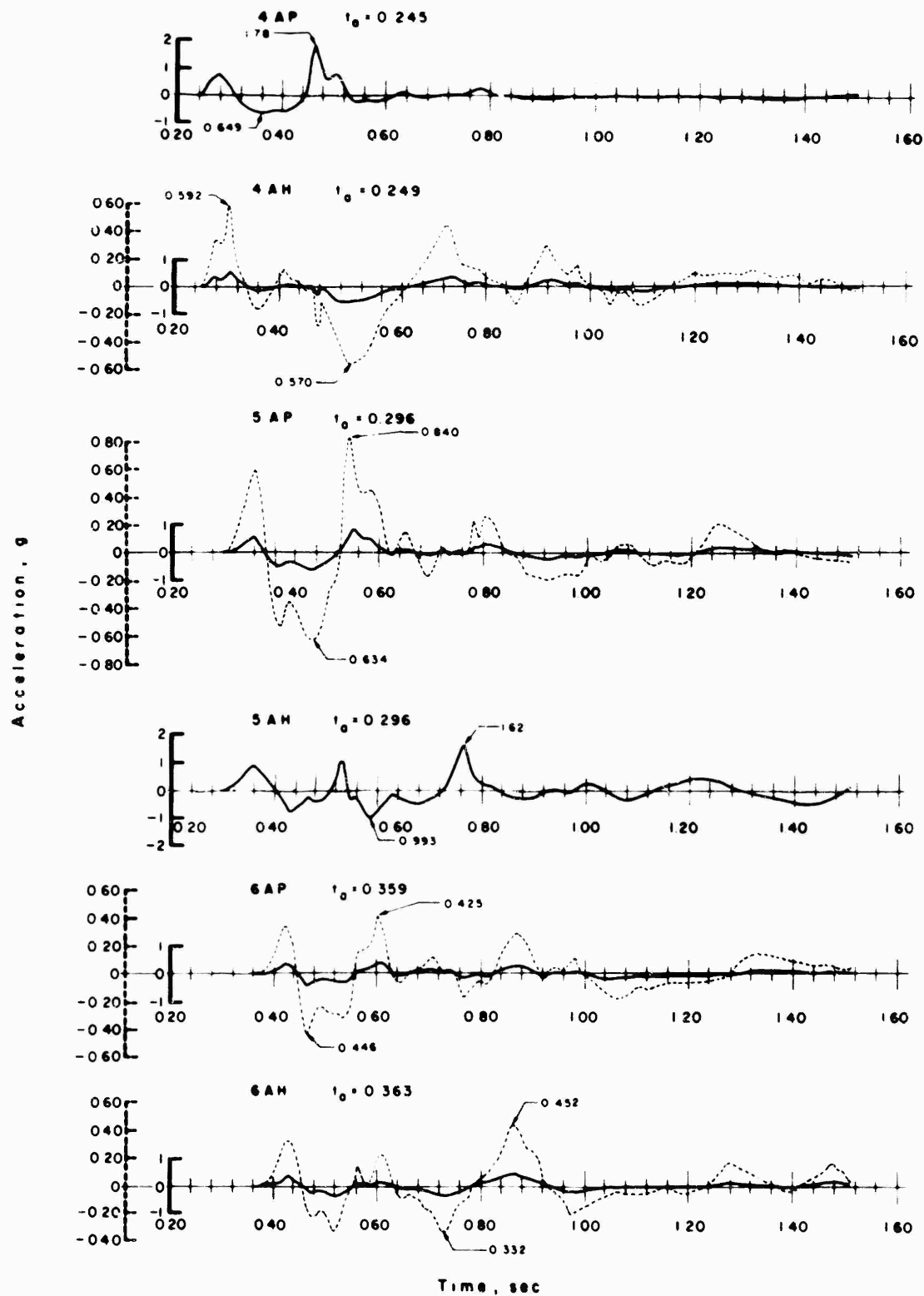


Figure 5.3 Vertical and horizontal acceleration, Stations 4, 5 and 6 (surface). (Broken line shows replot with ordinate scale increased by a factor of five.)

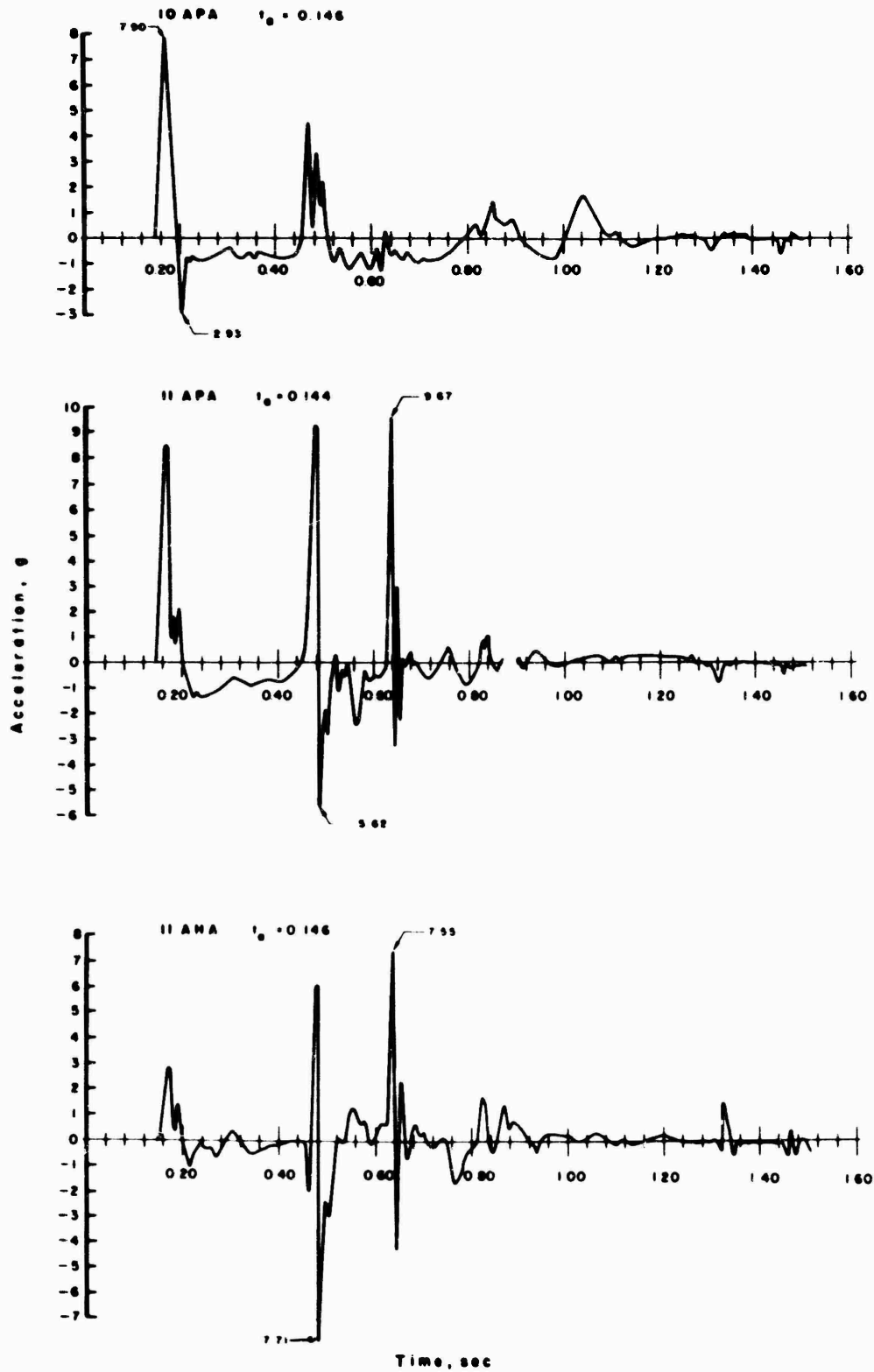


Figure 5.4 Vertical and horizontal acceleration, Stations 10 and 11 (slope).

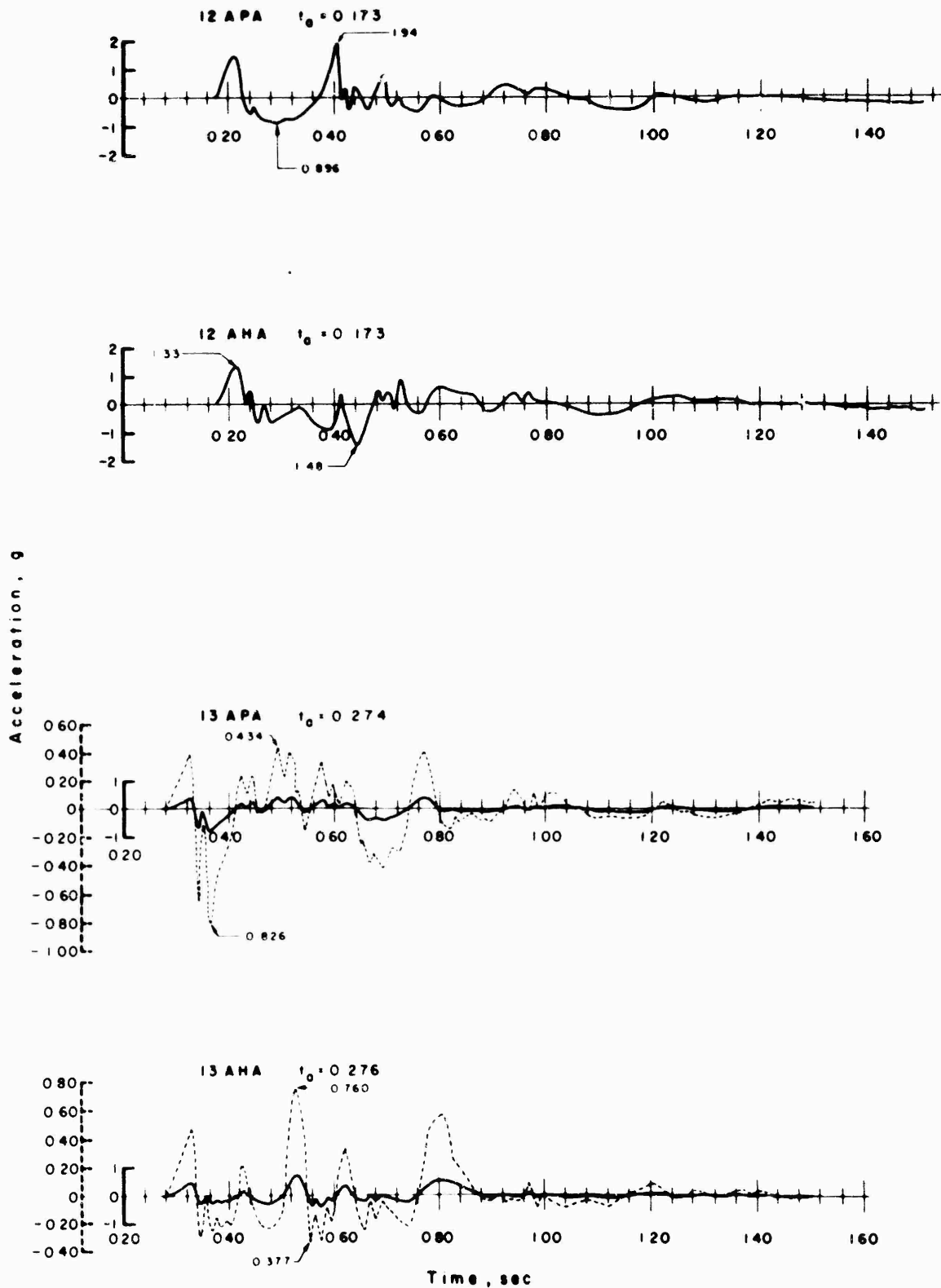


Figure 5.5 Vertical and horizontal acceleration, Stations 12 and 13 (slope).  
(Broken line shows replot with ordinate scale increased by a factor of five.)

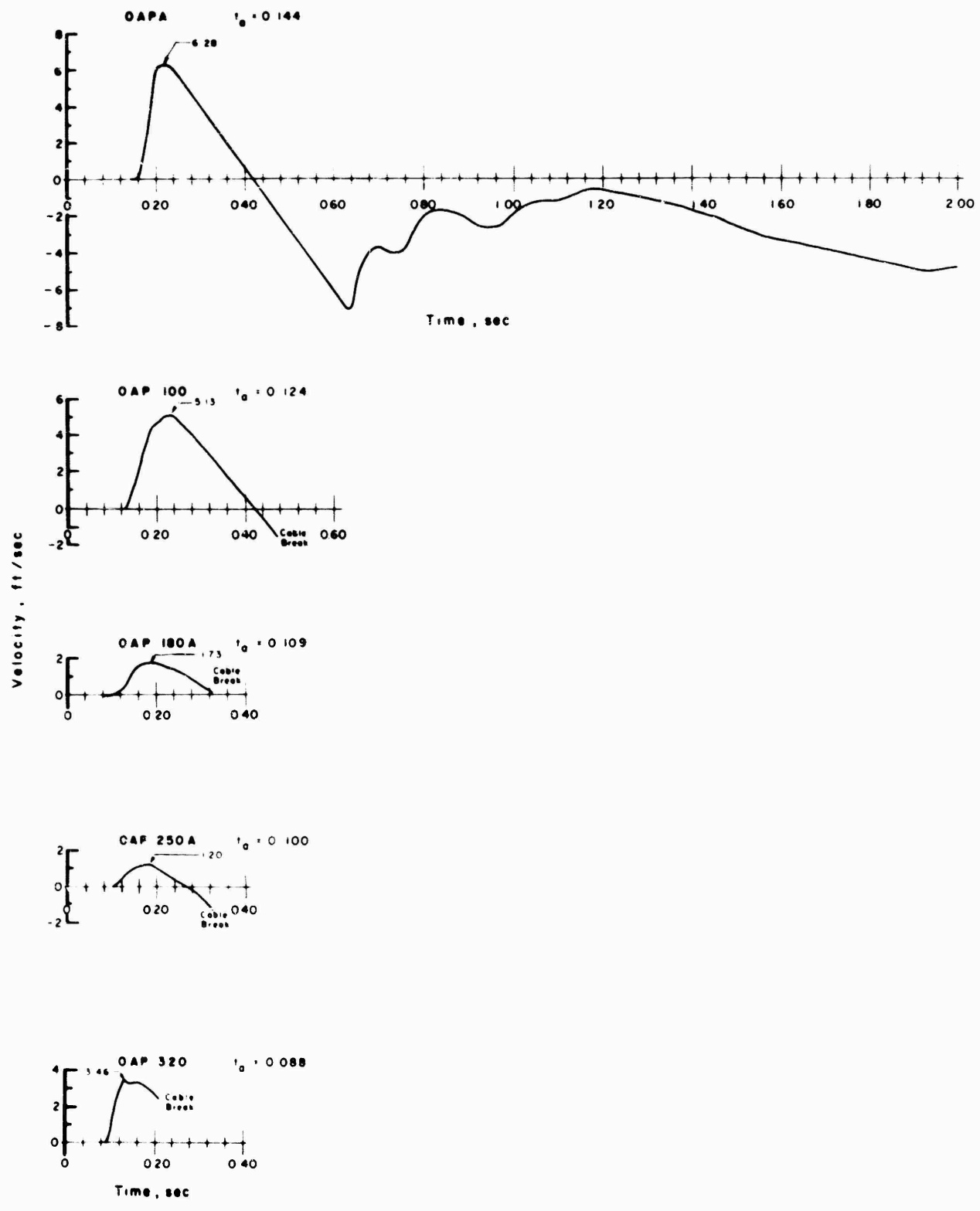


Figure 5.6 Vertical velocity, deep hole.

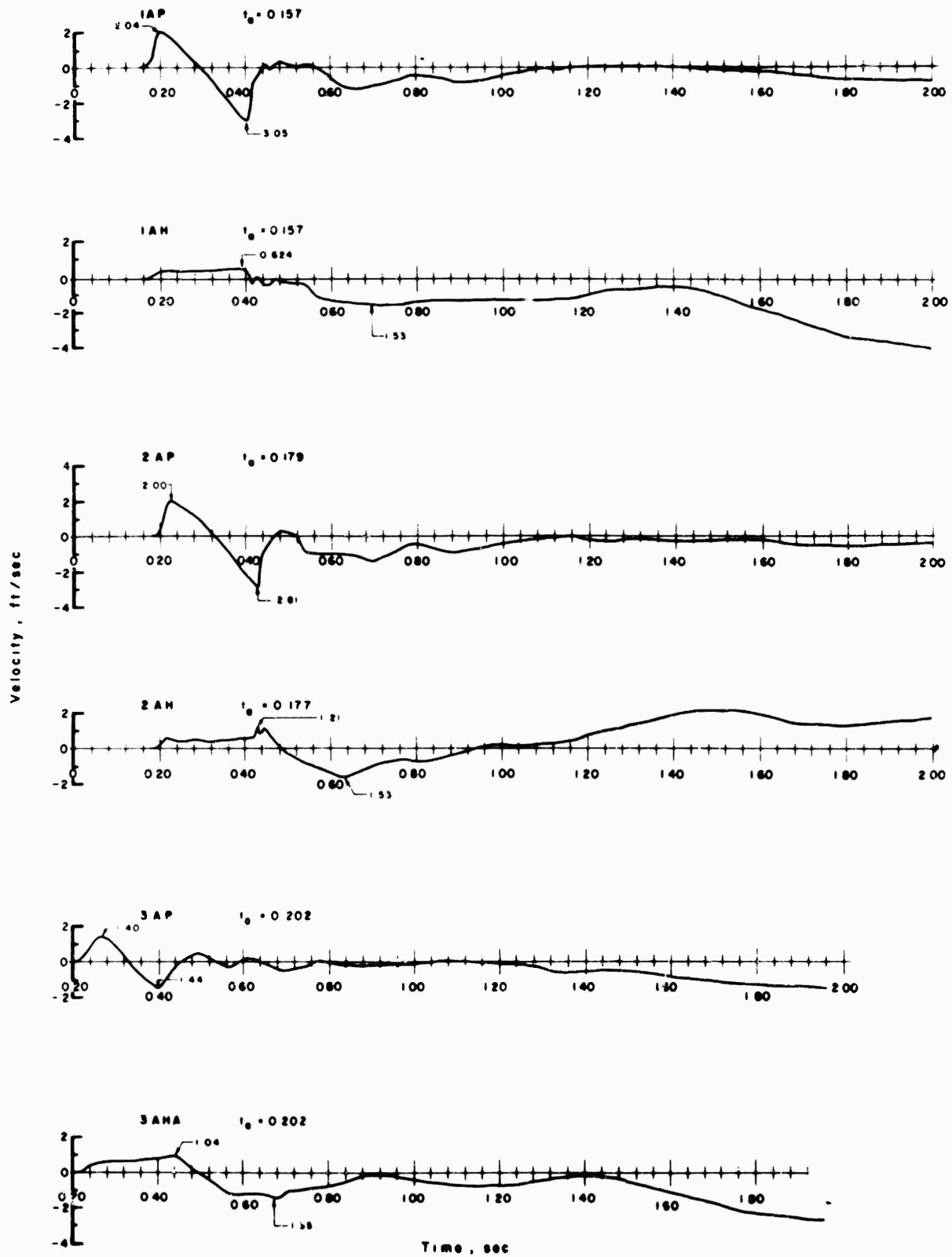


Figure 5.7 Vertical and horizontal velocity, Stations 1, 2 and 3 (surface).

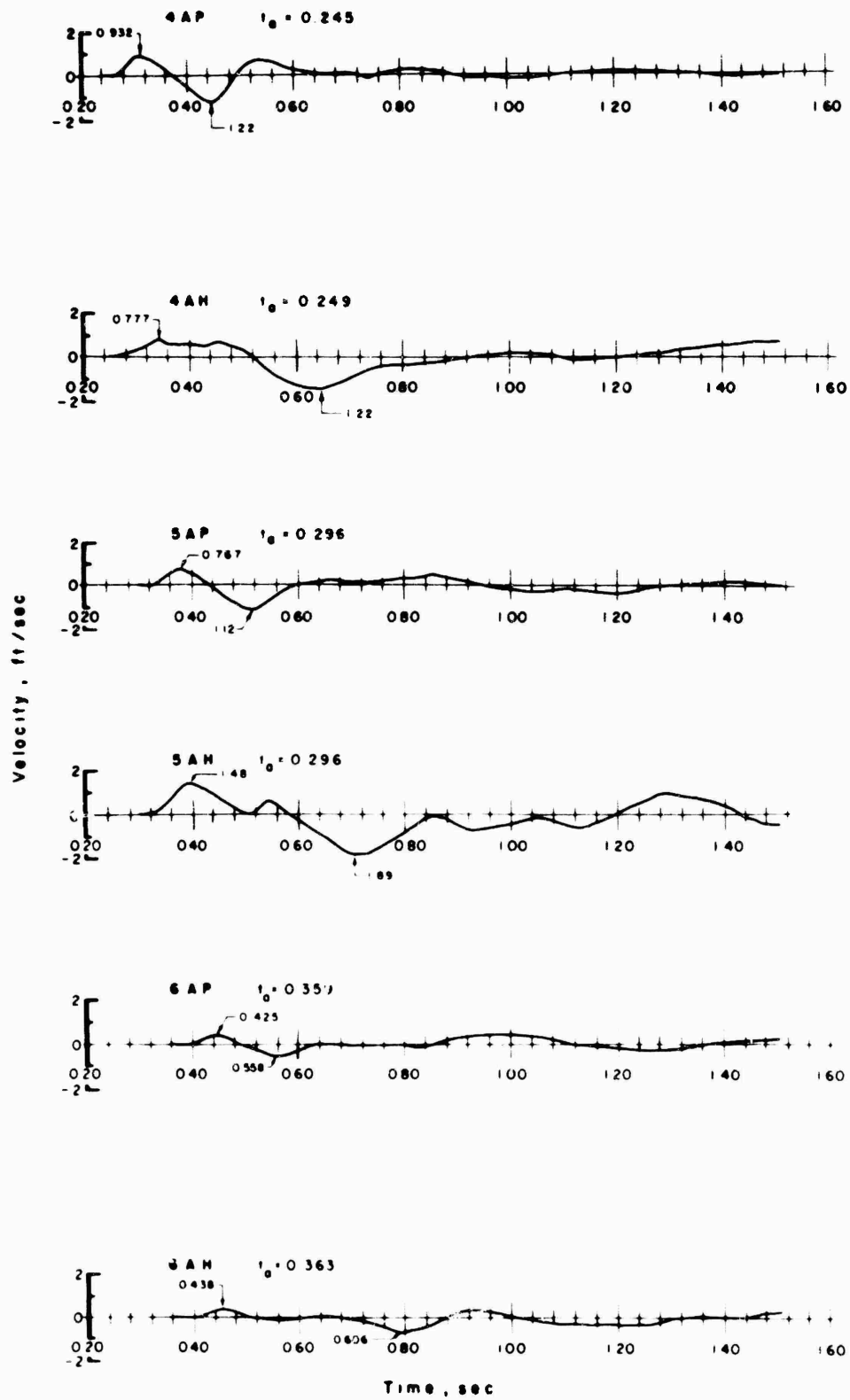


Figure 5.8 Vertical and horizontal velocity, Stations 4, 5 and 6 (surface).

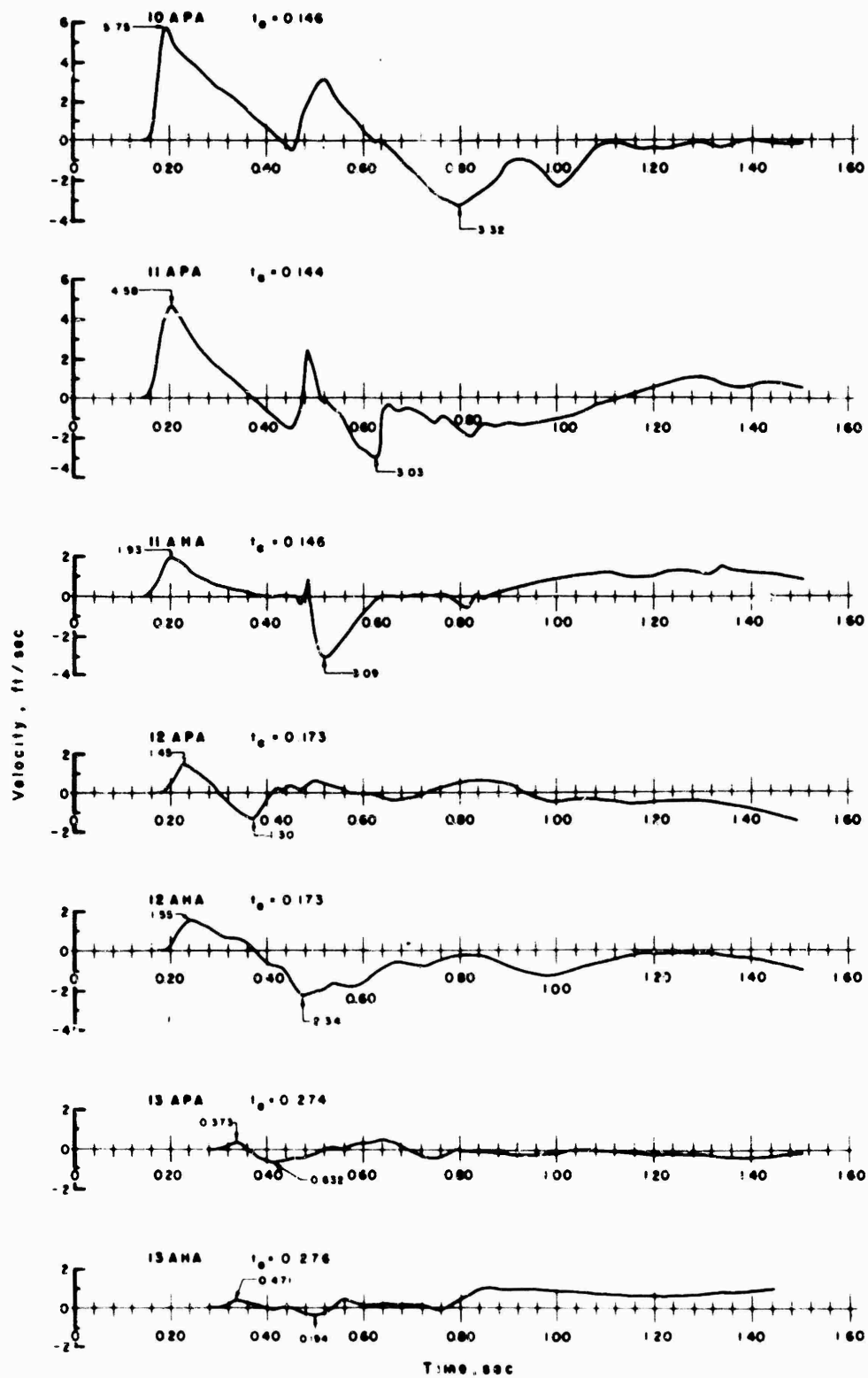


Figure 5.9 Vertical and horizontal velocity, Stations 10, 11, 12 and 13 (slope).

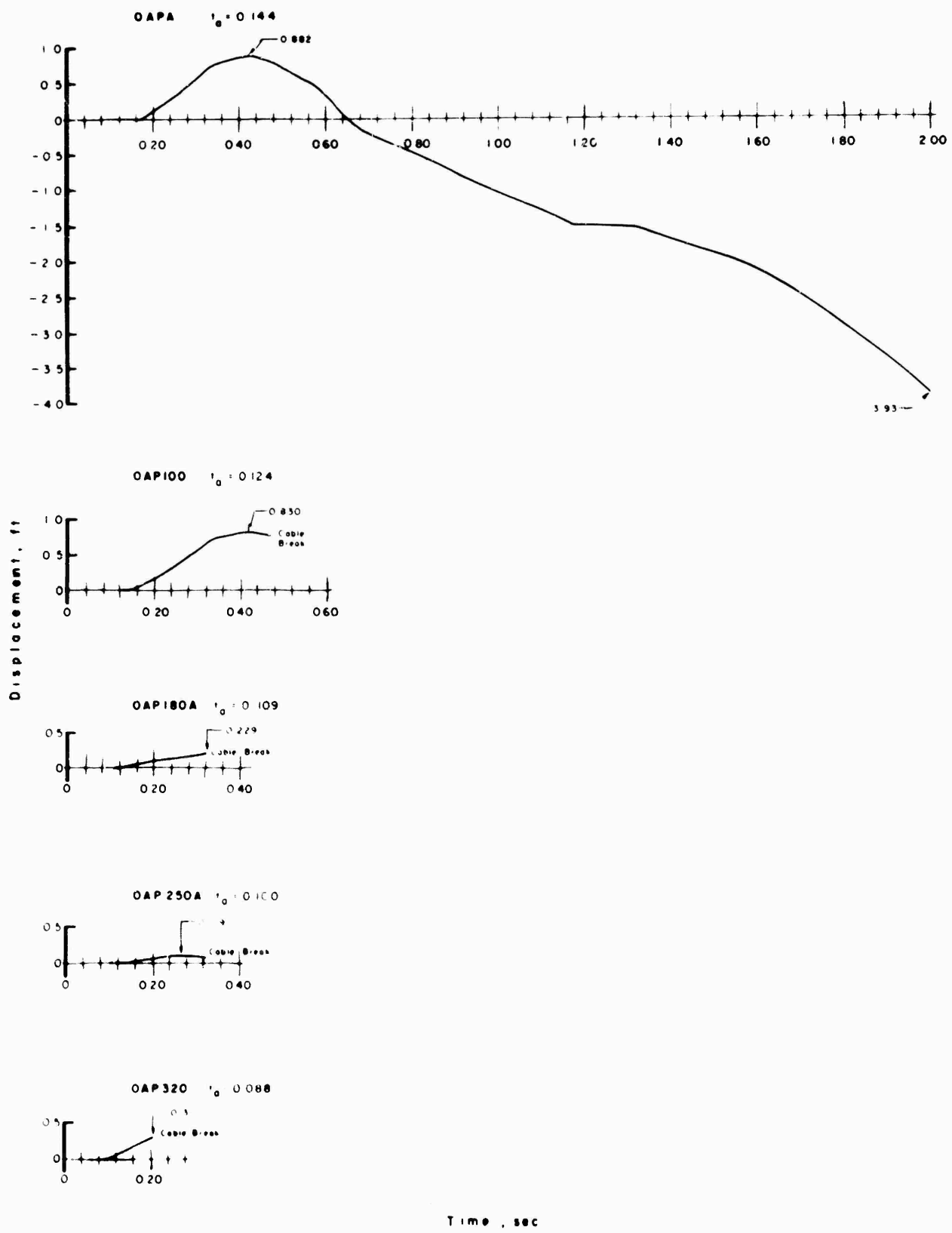


Figure 5.10 Vertical displacement, deep hole.

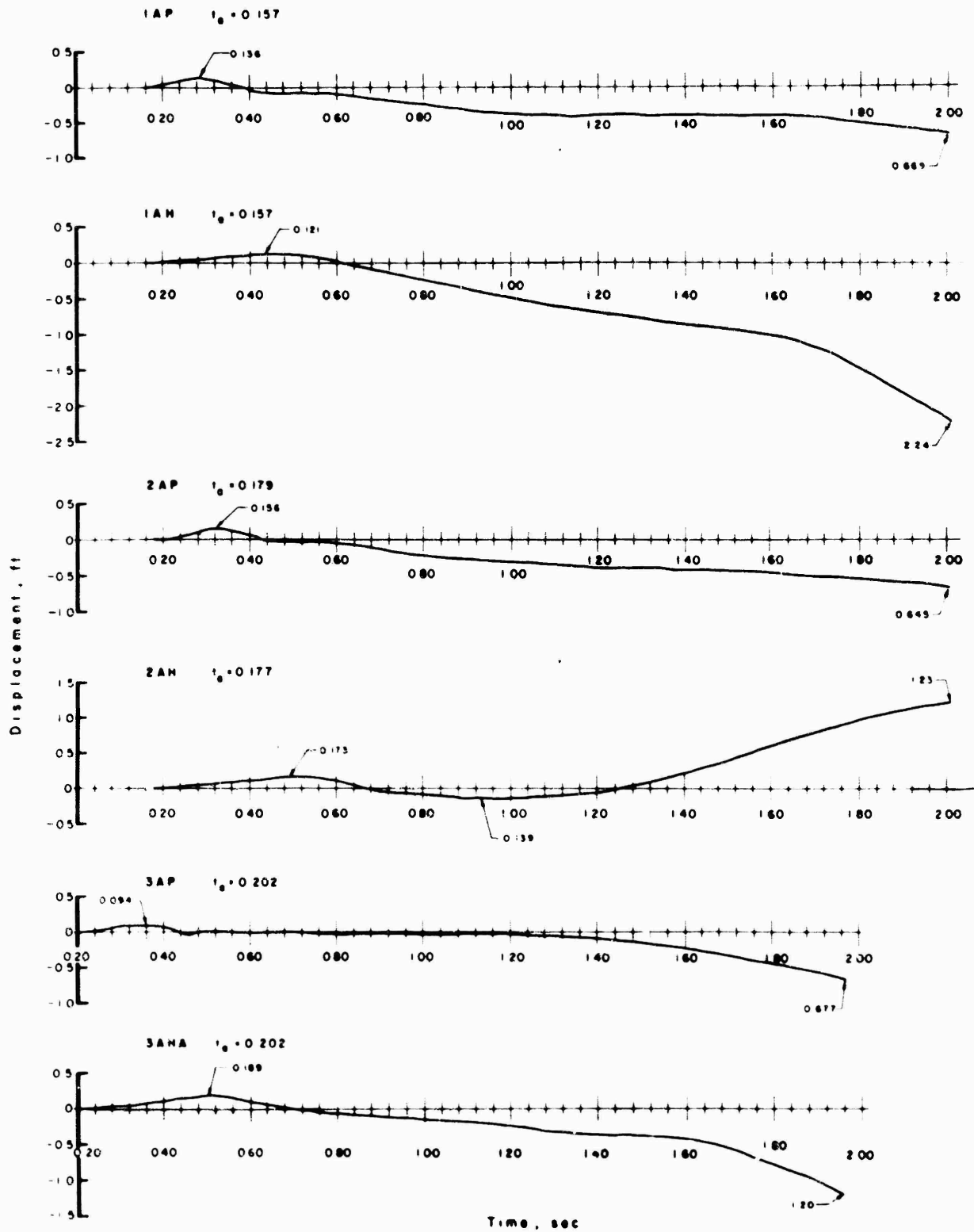


Figure 5.11 Vertical and horizontal displacement, Stations 1, 2 and 3 (surface).

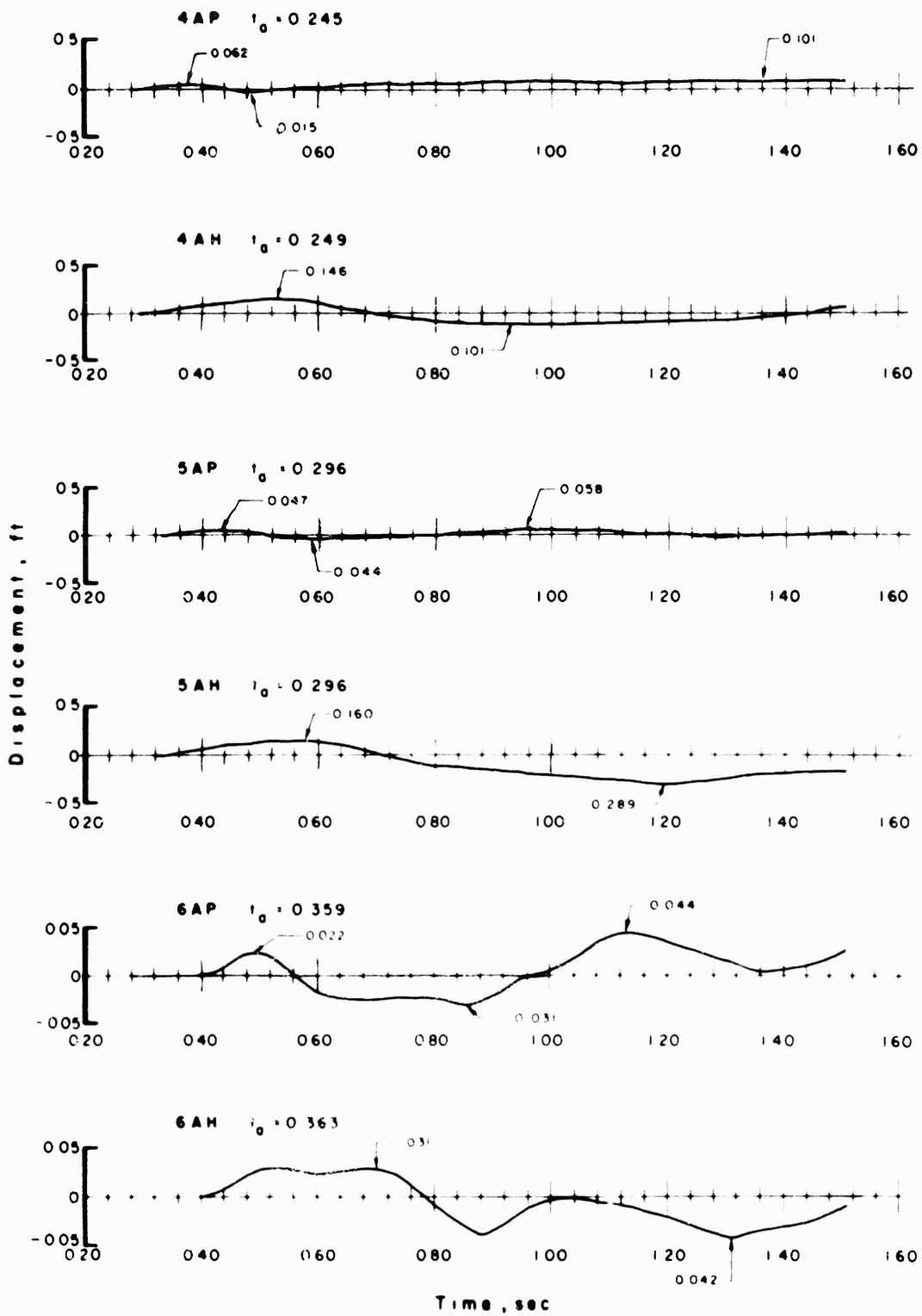


Figure 5.12 Vertical and horizontal displacement, Stations 4, 5 and 6 (surface).

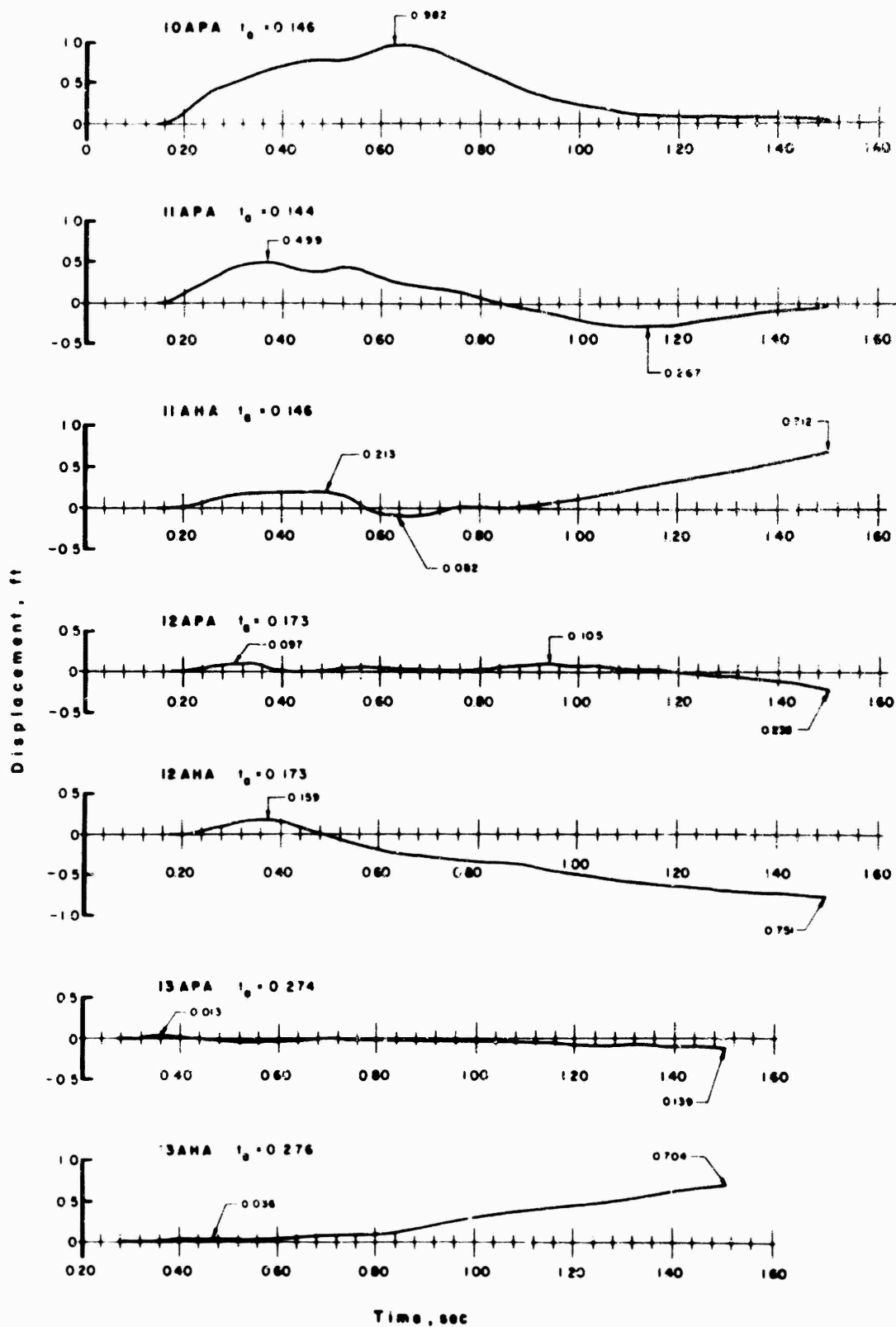


Figure 5.13 Vertical and horizontal displacement, Stations 10, 11, 12 and 13 (slope).

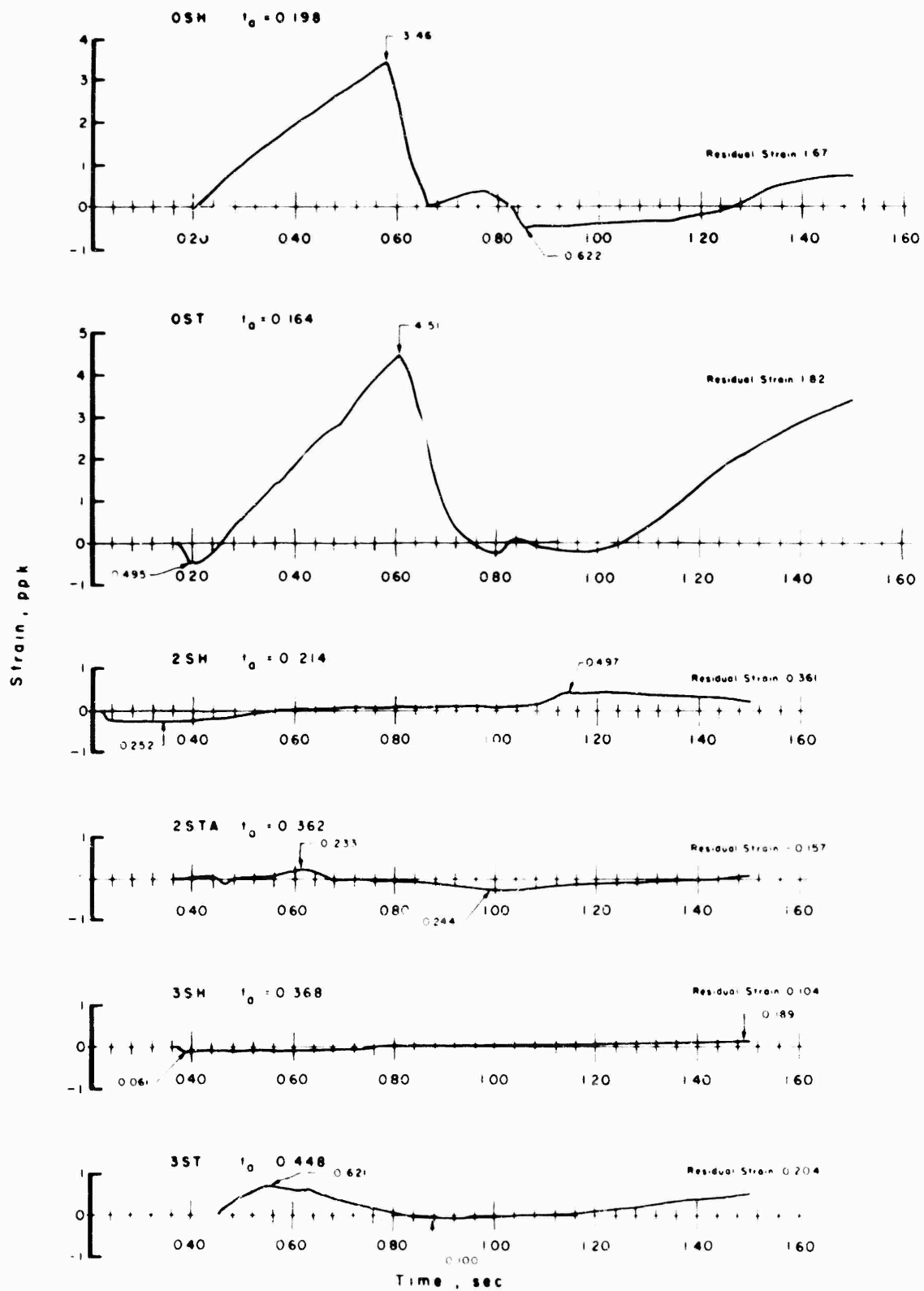


Figure 5.14 Horizontal and transverse strain, Stations 0, 2 and 3 (surface).

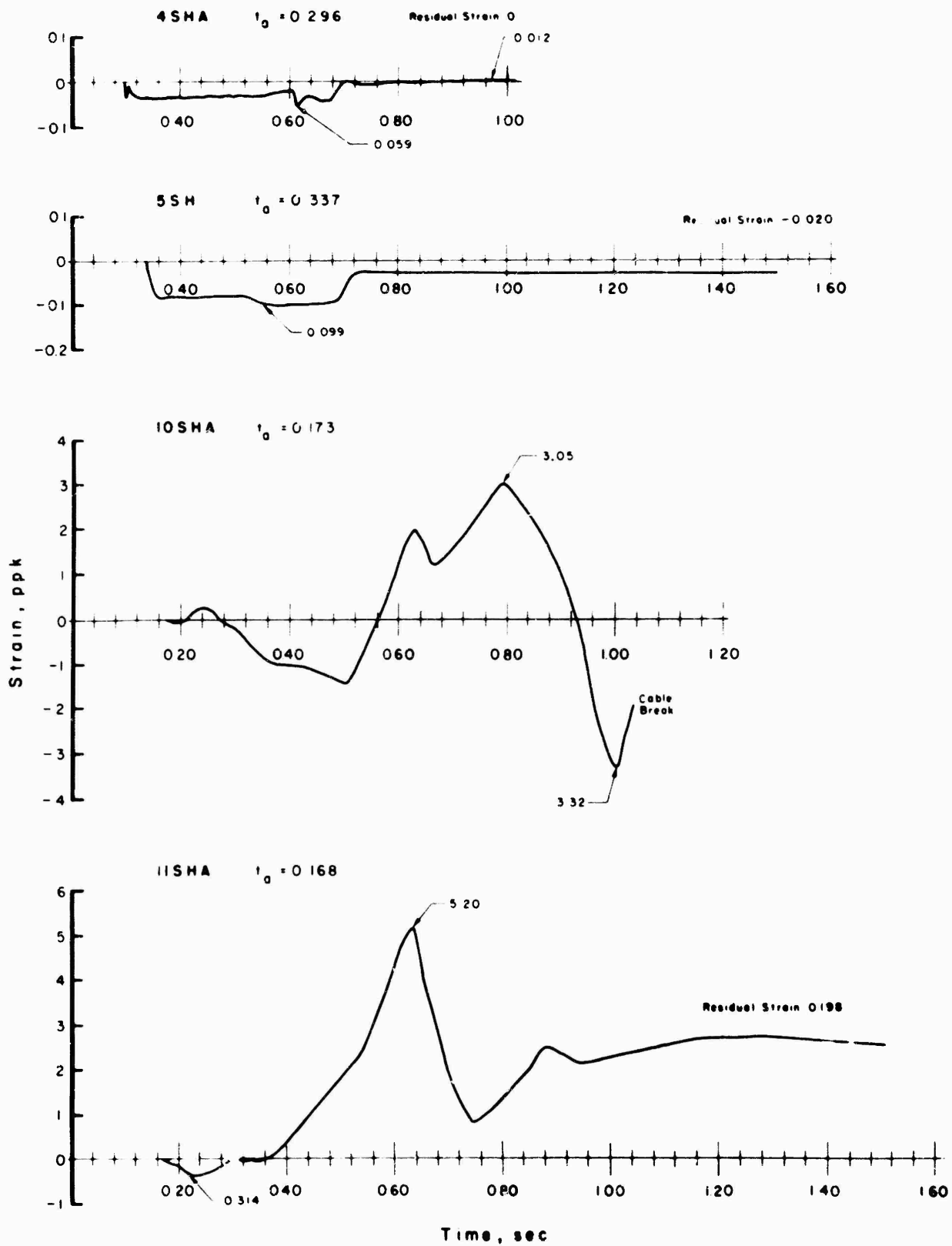


Figure 5.15 Horizontal strain, Stations 4 and 5 (surface), and Stations 10 and 11 (slope).

## CHAPTER 6

### DISCUSSION

The data of Project 26.4a will be discussed by phenomena in the following order: earth acceleration, velocity and displacement, seismic propagation velocities, and earth strain. The chapter ends with a brief discussion of the limitations of the instrumentation employed on the project.

#### 6.1 EARTH ACCELERATION

Acceleration data obtained in the deep hole near ground zero are shown in Figure 5.1, and the first peak vertical accelerations are plotted versus range from the explosion in Figure 6.1. It is noted that the data in Figure 6.1 has been plotted to A-scaled coordinates; that is, both the acceleration and the distance data have been reduced to conditions corresponding to a 1-kt-yield explosion detonated in the same medium.

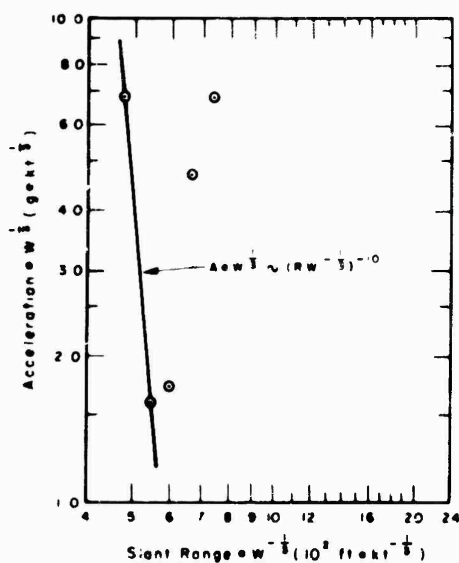


Figure 6.1 First peak vertical acceleration, deep hole, Rainier.

The figure indicates that the peak vertical acceleration decays sharply with distance from the charge between the two closest stations (i. e., 580- and 650-foot distances from the charge); however, at 180-foot depth and above there is a decided deviation from this regular behavior, with the peak acceleration at the surface registering more than 4 times that observed at 250-foot depth. Although cable breaks do not allow complete verification of the deep gage waveforms, the waveforms appear to follow the general pattern of the record obtained at the surface (OAPA) before the cables were broken. Although the acceleration peak recorded at the 320-foot depth was close to preshot prediction, the other measurements deviate markedly from the estimates. The observed severe decay of peak response with distance from the explosion (i. e., Figure 6.1 shows decay by a 10th power of the scaled radius) and the abrupt increase at the 100-foot depth were contrary to prediction. The decay equation is

$$A \cdot W^{1/3} = 3.3 \times 10^{27} (R \cdot W^{-1/3})^{-10}, \quad (6.1)$$

where A is in g-units, R is in feet, and W is in kilotons.

From the arrival times of the secondary acceleration peaks which follow the main peak (Figure 5.1), the following interval velocities are shown for the deep hole:

Gage depth ft	Arrival time of peak sec	Interval velocity ft/sec	Arrival time of peak sec	Interval velocity ft/sec
0	---	---	0.184	5,000
100	0.204	2220	0.204	5,720
180	0.168	7000	0.218	11,700
320	0.146	5830	---	---

The secondary peak seen on the OAP320 record at 0.146 second is also evident on the OAP250 and OAP180 records, yielding interval seismic velocities which are reasonable for the Oak Springs tuff. However, the secondary peak on the OAP100 record is probably not identified with this same disturbance--the interval velocity is too low (2220 feet per second). To be identified with the same disturbance, the peak should arrive at about 0.185 second at the 100-foot deep gage.

This second peak (i. e., arrival at 0.204 second) on the OAP100 record is consistent with the arrival of a downward-traveling reflected wave from

the surface. The reflected wave can also be identified at the 180-foot deep station. But the peak at 0.224 second on the OAP250 record does not fit with this reflected energy traveling downward--the interval velocity is too high (11,700 feet per second). This peak is probably from another secondary disturbance from the explosion; however, due to the cable break, it is not possible to confirm this on the OAP320 record.

As explained in Section 2.2.3, the reflected stress wave is a tension wave (negative stress) traveling downward; this will produce the positive (upward) acceleration observed on the OAP100 and OAP180 records. Although the incident compression wave and the reflected tension wave at the surface coincide in time and produce together a single acceleration pulse, at 100-foot depth the tension peak should lag the compression stress maximum by the length of time it takes a stress wave to travel to the surface and return. The OAP100 and OAP180 records are consistent with this explanation. Furthermore, it is concluded that, since no peak identifiable with the reflected energy is noted at the expected times at 250- or 320-foot depths, the earth may have parted somewhere below the 180-foot depth; moreover, it appears that the wave was destroyed by the fracture since no additional reflections are evident.

Assuming that the earth, as a jointed medium, can not support tension suggests that the fracture must occur at the depth at which the tensile stress (in the wave reflected from the surface) is just equal to the overburden pressure (called the "critical depth"). However, in general this simple rule does not hold. The actual conditions for fracture will depend upon the wave length of the disturbance, as illustrated in Figure 6.2 representing a rod and an ideal rectangular pulse. With a short-wave length, tension failure may occur to depths shallower than critical; however, with a long-wave length, the time of fracture is determined by the arrival at the critical depth of the trailing edge of the pulse. The time of fracture is controlled by the arrival of the leading edge of the reflected wave only when the wave length is less than twice the critical depth. If one considers nonrectangular stress pulses (i.e., the waveforms of Figure 5.6), the picture of Figure 6.2 is not changed considerably; there would be a tendency for failure to occur at somewhat shallower depths than predicted for rectangular pulses.

If this explanation of fracture is correct, an additional observation is pertinent. As the yield of the device increases, the stress wave is longer in time and space. If the wave length of the stress wave is less than twice

the critical depth, the depth of the fracture will increase as the size of the experiment is increased (Figure 6.2). However, if the wave length is longer than this value, then failure will always occur at the critical depth. Sandia data (Reference 11) show that Rainier stress wave lengths are about equal to the depth of burial of the charge. Therefore, failure will occur at the critical depth regardless of wave intensity. If the stress intensity increases when the scale of the experiment increases, then the critical depth will increase and so will the depth of fracture.

On a scaled basis, the peak stress should be the same at the same scaled distance from the charge, if the medium "scales" according to conventional criteria. However, when free surfaces or earth strata are introduced, leading to reflections and refractions of the explosive energy, predictions based upon scaling criteria become nebulous. Thus, although it can be concluded that the depth at which the "cap-lifting" fracture occurs will probably increase as the scale of the experiment increases, it does not follow directly that this can be used as a firm criterion for containment of the explosion. More data from future deep underground detonations are necessary before the degree of containment can be predicted with confidence.

From the vertical acceleration measurements made on the surface (Figures 5.1, 5.2, and 5.3), the following facts become evident:

1. The gage records, particularly out to 650-foot range, are of the same general appearance, i. e., an initial positive (upward) acceleration peak followed by a long negative phase and then another positive peak.
2. The initial acceleration pulse is identified with the motion of the overburden due to the detonation energy arriving at the ground surface. It will be noted that generally the negative phase amplitude (OAP, 1AP, 2AP, and 3AP) is approximately 1 g; This suggests that the earth surface at these radii was thrown up and was subsequently in free fall for several tenths of a second. There is evidence that there was a separation of the earth medium at some depth, a fact which will be verified when particle velocity and displacement are discussed (Section 6.2).
3. The second acceleration pulse is interpreted as the bottoming of the surface section as it fell back onto the main mass of the mesa. The shock pulse must have been initiated at the contact interface at depth and then transmitted to the surface.

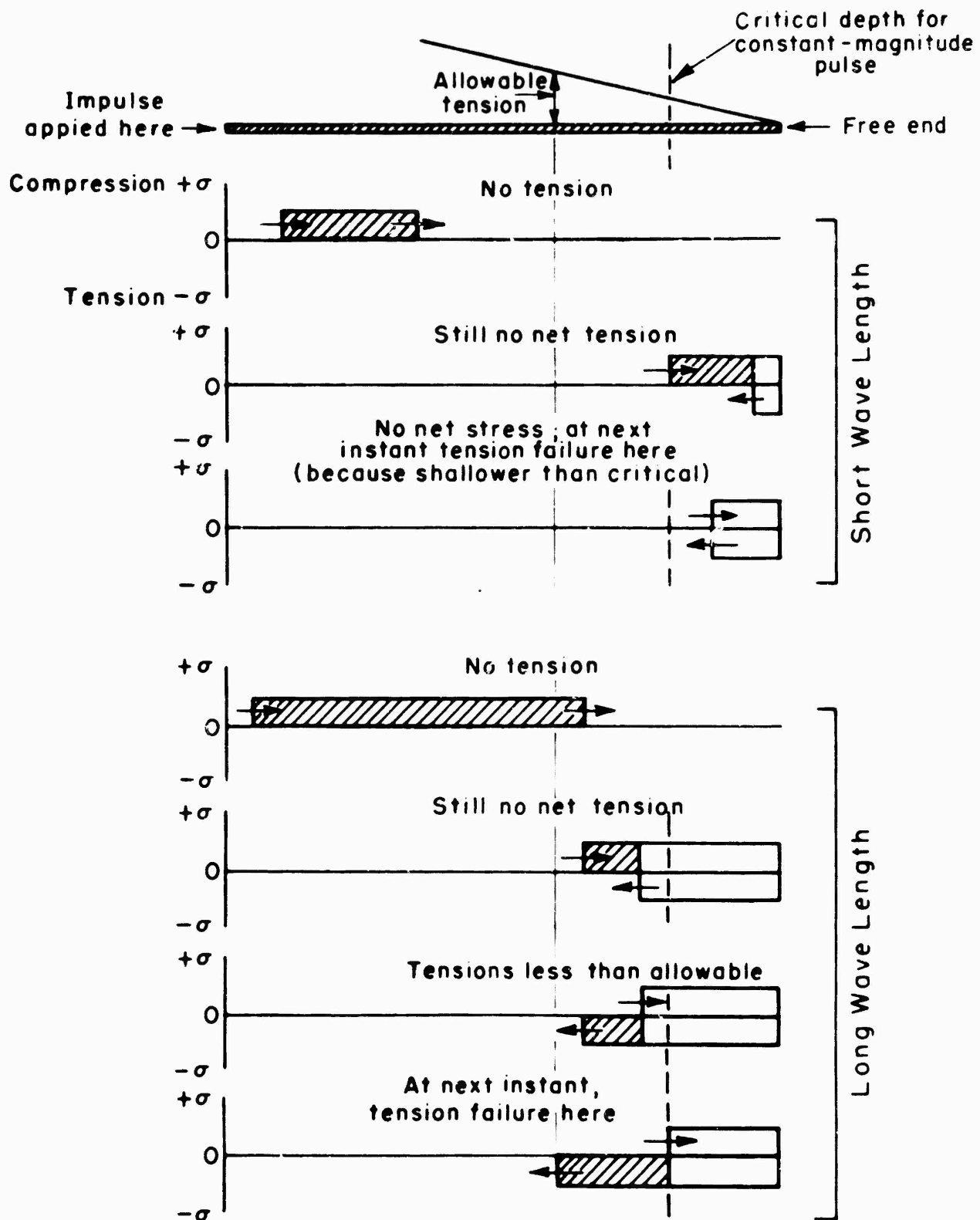


Figure 6.2 Schematic diagram of the effect of wave length on tension failure.

ERRATUM TO REPORT WT-1528

SURFACE MOTION FROM AN UNDERGROUND DETONATION

equation (6.2), page 51, should read:

$$AW^{1/3} = 8.5 \times 10^9 (R/W^{1/3})^{-3.2}$$

rather than

$$A \cdot W^{1/3} = 3.5 \times 10^9 (R \cdot W^{-1/3})^{-3.2}$$

4. The region around Station 1 bottomed considerably before that around Station 0 and slightly before that at Station 2 (Figures 5.1 and 5.2). This time interval between Stations 0 and 1 is so great that there must have been a serious fracture between these gage stations so that two separate pieces of material fell back. This conclusion is substantiated by the 11APA record (Figure 5.4) which shows evidence of two distinct bottomings of approximately equal intensity.

The multiple peaks associated with the second main acceleration pulse (Figures 5.3 and 5.4) are probably due to reflections of the second pulse near the surface. The fact that the reflections appear so regular at some of the stations (especially Station 1AP) makes attractive an analysis of the records to determine the source of the disturbances.

The acceleration records at many stations seem to show a sharper (and larger) shock when the blocks of rock bottomed than when they were thrown up. This can be explained by the fact that the block probably moved up with the moving substratum before separation occurred; however, when the block returned and bottomed, the substratum had fallen somewhat and was more nearly stationary. Thus, the time of stopping would have been much shorter than the time of starting; i. e., if the two impulses were equal, the bottoming force (or acceleration) would be the larger.

The A-scaled maximum vertical acceleration (first peak) is plotted as a function of A-scaled slant range (or radial distance) in Figure 6.3. The figure indicates that, out to an A-scaled range of about 1500 feet, the peak vertical acceleration decays according to the inverse 3.2 power of the range. The equation is

$$A \cdot W^{1/3} = 3.5 \times 10^9 (R \cdot W^{-1/3})^{-3.2}, \quad (6.2)$$

where A is in g-units, R is in feet, and W is in kilotons.

Figures 5.1 through 5.3 indicate that the conclusions about the vertical measurements are reinforced by the horizontal results. The horizontal acceleration records at Stations 1 and 2 (1AHA and 2AH) shown virtually zero radial acceleration of the earth cap during the period between initial peak and bottoming response, which confirms the idea of free-fall; also, the time of free-fall indicated on these records is consistent with the vertical records. At both stations, the initial upward acceleration pulse contained a radial component directed away from ground zero; also, the horizontal records

indicate that the earth cap containing Stations 1 and 2 bottomed before the cap containing Station 0.

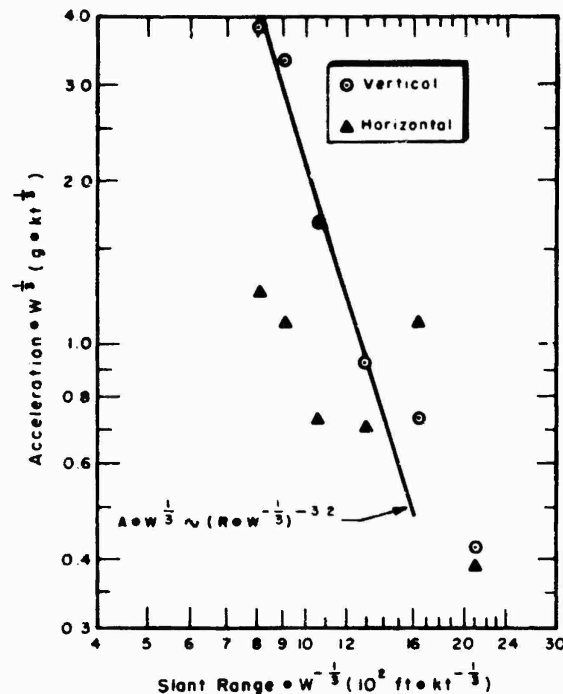


**Figure 6.3 First peak horizontal and vertical acceleration, surface level, Rainier.**

The first peak horizontal acceleration plotted on Figure 6.3 indicates that at the closer ranges the horizontal component was markedly less than the vertical. However, beyond A-scaled ranges of 1200 feet the two components are more comparable, with the horizontal even exceeding the vertical at one range.

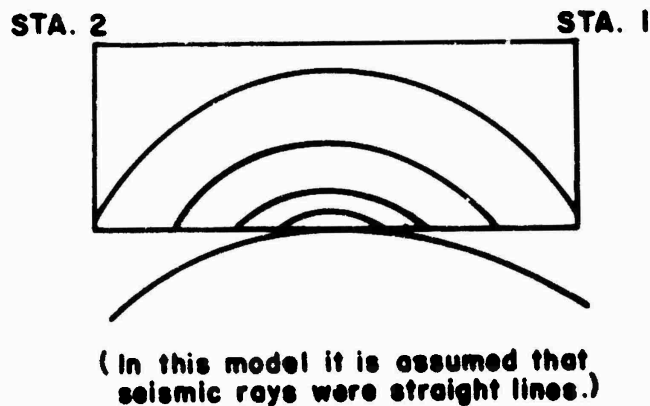
The horizontal accelerations produced by the elastic wave which travelled from the plane of impact to the surface show several fluctuations between positive and negative, which were produced by multiple reflections from planes at shallow depths. These reflections do not agree in form and in arrival time with the reflections recorded by vertical accelerometers at the same stations. It is possible that the (really minor) disagreements in arrival times and sign

of the reflected waves which were recorded between 0.4 and 0.5 second on 1AH, 1AP, and 2AH, 2AP are due to the fact that 1AH and 2AH were recording shear waves, while 1AP and 2AP were recording longitudinal waves. An explanation based on this possibility would go on to say that since shear waves travel more slowly than longitudinal waves, even if they were reflected from the same depth, they would arrive later. However, since the reflection of the longitudinal waves from two or three depths would produce a pattern of arrivals of these reflections which is not simple, this explanation is discarded. Furthermore, the arrival of a longitudinal plane wave at Stations 1 or 2 could produce horizontal as well as vertical accelerations, provided the plane of the wave is inclined to the horizontal.

Plane longitudinal waves reflected from various depths could easily arrive in planes inclined to the horizontal, and almost any combination of positive and negative horizontal accelerations can be arranged for by only moderate changes in the geometries of the reflecting surfaces. For example, the first pulse that arrived at 1AH from the bottoming was a radial acceleration towards ground zero, while at 2AH the first pulse was radially away from ground zero. This can be explained by the geometry of sketch C below; that is, by the assumption that bottoming was really achieved at first only at the center of the bottom of the cap to which the gages were attached.

On April 5, 1958, one of the world's largest man-made nonnuclear explosions was fired at Ripple Rock in Seymour Narrows on the west coast of Canada (Reference 12). The object of the explosion

was to remove a twin-peaked underwater rock from the center of a narrow seaway. The method adopted was to sink a 500-foot shaft on a nearby island and drive a 2400-foot tunnel to points beneath the peaks. Additional shafts, each 300-feet high, were driven upward into the rocks and, an extensive system of short tunnels was excavated to honeycomb the peaks. These tunnels were filled with 1400 tons of "Nitramex 2H" (DuPont and Co. of Canada). Peak accelerations measured on the surface gave the following results:



Sketch C

(a) From slant ranges of 400 to 2000 feet (A-scaled), the peak vertical accelerations obey the relation

$$A \cdot W^{1/3} = 1.73 \times 10^9 (R \cdot W^{-1/3})^{-3.0} \quad (6.3)$$

(b) The horizontal components of acceleration (peak outward) are consistently less than the vertical at closest stations, and are comparable to vertical beyond 2000 feet A-scaled.

(c) Beyond 2000 feet, principal motion is in and down.

(d) The seismic velocity of the local basalt is about 15,000 feet/sec.

(e) An estimate of the seismic energy made from the records gave about 0.2% of the total, based upon  $4 \times 10^{16}$  ergs per ton of explosive.

Comparing Eqs. 6.2 and 6.3, it is evident that the decay of peak vertical acceleration with distance is not significantly different for Rainier and Ripple Rock. However, the constant in the equation is larger for Rainier; probably more than the 0.2% of the total went into seismic energy for Rainier. If one assumes that the peak surface accelerations are sufficiently indicative of this fraction of the energy going into the seismic wave,

$$\frac{8.5 \times 10^9}{1.73 \times 10^9} \times 0.2 \cong 1\%$$

can be calculated for Rainier.

The acceleration measurements taken on the slope line for Rainier are summarized in Table 5.1, and the first peaks are plotted in Figure 6.4. Also included in the figure for comparison is the surface level vertical acceleration curve of Figure 6.3.

Before discussing the results of these measurements, it should be noted that the labels "vertical" and "horizontal", when applied to the slope line gages, mean vertical or horizontal with reference to the terrain in the vicinity of the gage mount. Therefore, any comparisons between the mesa surface results and those obtained on the slope will necessarily be only qualitative. It also is pertinent that both the surface and slope measurements were taken on the cap rock (welded tuff), rather than in the unconsolidated tuff in which the explosion was detonated.

Figure 6.4 indicates that the vertical peaks of acceleration on the slope are somewhat larger close-in than on the mesa, but at the larger ranges the slope line peaks fall below the mesa curve. Also, close-in the horizontal peak is notably lower than the vertical, while the vertical and horizontal are

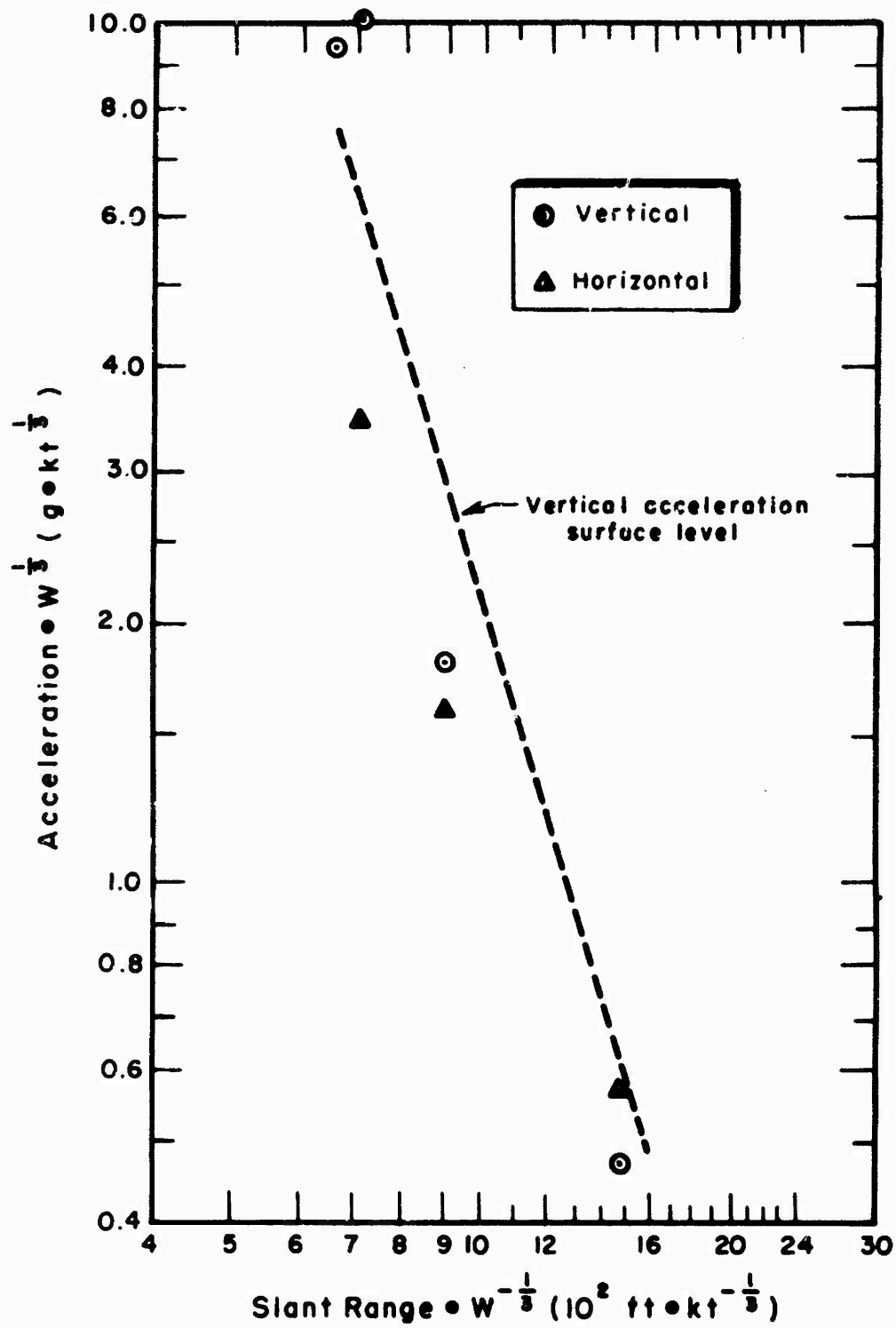


Figure 6.4 First peak horizontal and vertical acceleration, slope line, Rainier.

comparable farther out. However, these differences between the peak accelerations measured on the Rainier mesa surface and on the slope are not large enough to be significant.

## 6.2 EARTH PARTICLE VELOCITY AND DISPLACEMENT

Machine integration of the acceleration-time records to obtain earth velocity and displacement yields the results listed in Tables 5.2 and 5.3.

6.2.1 Particle Velocity. The results of the integration of the deep hole acceleration records are summarized in Figure 6.5. From the figure, it is apparent that the earth formation parted (fractured) at a minimum of two depths. Looking at the velocity-time curves at a time of 0.30 second, the velocity corresponding to the surface and 100-foot depth is large and positive; the 180-foot depth value is notably smaller and positive, and the 250-foot depth velocity is negative. This suggests that the earth parted between 100- and 180-foot depths and between 180- and 250-foot depths. These data do not preclude the possibility of other fracture planes at other depths. In fact, the differences in velocity-time curves associated with the surface and 100-foot depth stations, because the maxima are unequal, suggest a fracture between zero and 100-foot depth.

Figure 6.6 presents the first peak vertical velocity as measured in the deep hole over the charge. The initial decay of peak velocity with A-scaled slant range obeys the equation,

$$V = 2.5 \times 10^{27} (R \cdot W^{-1/3})^{-10} . \quad (6.4)$$

It should be noted that if the cap rock (welded tuff) in the vicinity of ground zero is 250- to 274-feet thick, then it is probable that the OAP320 gage is located in softer material than is the OAP250 gage.

Wave theory gives the following formula for particle velocity at the interface between two materials after passage of a step pulse:

$$V = \frac{\sigma}{\rho_1 C_1} \frac{2}{1 + \frac{\rho_2 C_2}{\rho_1 C_1}} \quad (6.5)$$

where  $\sigma$  is the stress change across the approaching wave front,  $\rho_1 C_1$  is the impedance of the material in front of the interface, and  $\rho_2 C_2$  is the impedance beyond the interface. The step velocity across the approaching front is

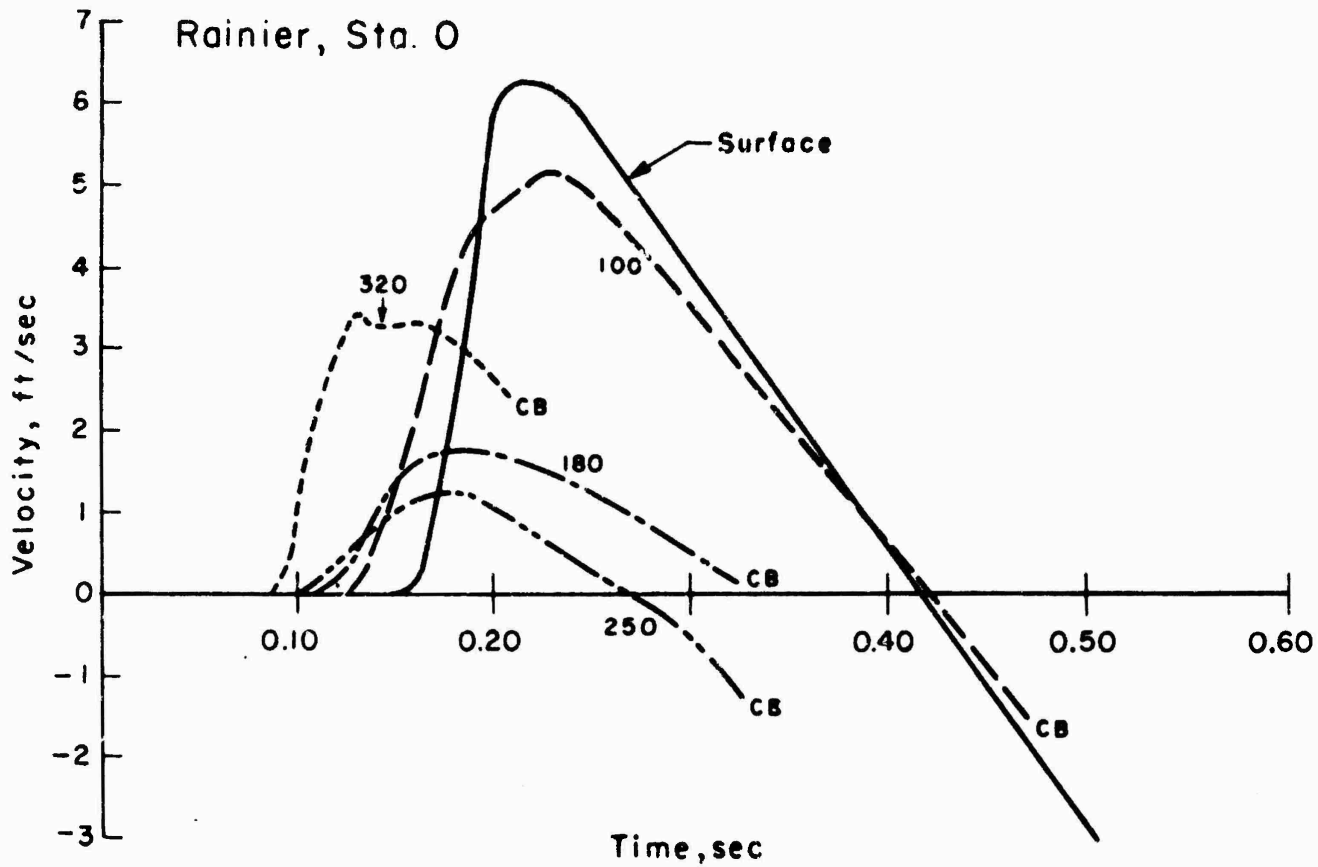


Figure 6.5 Earth velocity vs time, deep hole, Rainier. (CB - cable break.)

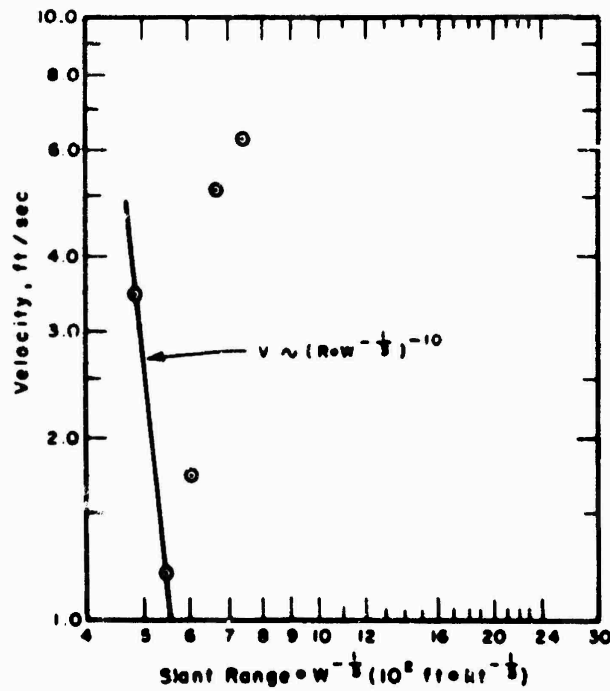


Figure 6.6 First peak vertical velocity, deep hole, Rainier.

$$V = \frac{\sigma}{\rho_1 C_1} \quad (6.6)$$

Thus, the theory suggests the following two rules:

1. If an accelerometer is located at or near the transition from a hard to a soft material, the size of the peak acceleration is increased (because the particle velocity jump is increased).
2. If an accelerometer is located at or near the transition from a soft to a hard material, the peak acceleration is diminished (because the particle velocity jump is decreased).

This analysis explains partially the very large negative exponent found in Equations 6.1 and 6.4. Because of the presence of the abrupt change in rock characteristics near 250-foot depth at the Rainier mesa site, one is loathe to generalize the Project 26.4a vertical hole results for prediction of the effects for future tests in different areas. The surface level measurements would also be affected by the layering character of the area, but to a much lesser extent.

The surface level peak horizontal and vertical velocity data are plotted in Figure 6.7. The vertical velocity curve shown follows the equation

$$V = 9.7 \times 10^4 (R \cdot W^{-1/3})^{-1.6} \quad (6.7)$$

Peak horizontal velocities on the surface are generally much lower than the vertical close-in, are comparable at mid-ranges, and are possibly higher beyond 1500 feet (A-scaled). The Rainier vertical velocity decay with slant range compares favorably with the Ripple Rock (Reference 12) results, which approximate the equation

$$V = 5 \times 10^3 (R \cdot W^{-1/3})^{-1.5} \quad (6.8)$$

These equations indicate that peak velocity magnitudes on Rainier, at comparable scaled ranges, are about twenty times larger than those recorded at Ripple Rock. Part of this large divergence can be traced to the fact that the Ripple Rock explosion was not confined and was detonated in a more competent material.

The velocity data obtained on the Rainier slope line are presented in Figure 6.8; also included is the curve of the peak vertical surface velocity from Figure 6.7. Only at the closest slope line station is the peak velocity higher than that measured on the surface; the remaining horizontal and vertical peak values fall below the mesa curve.

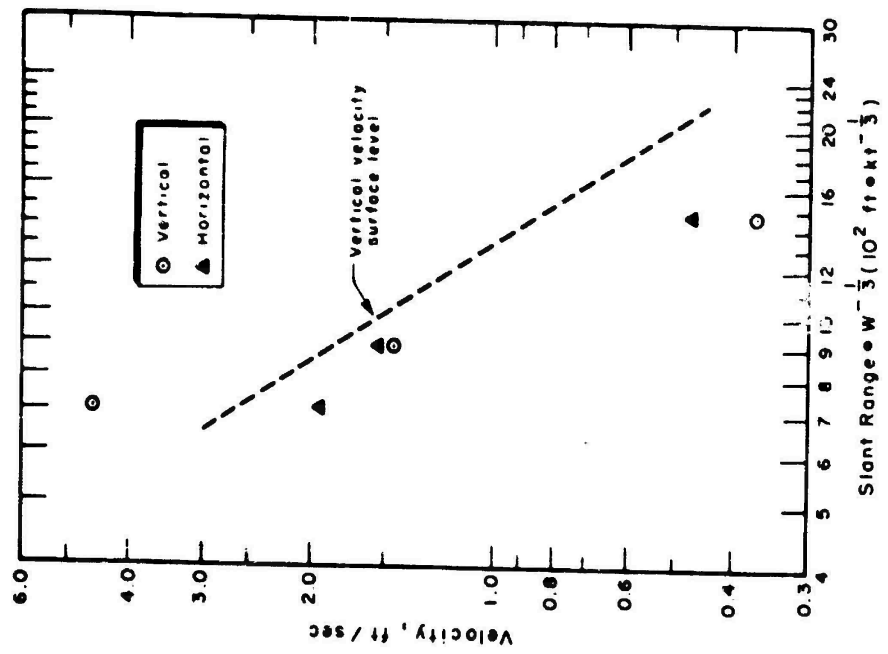


Figure 6.7 First peak horizontal and vertical velocity, surface level, Rainier.

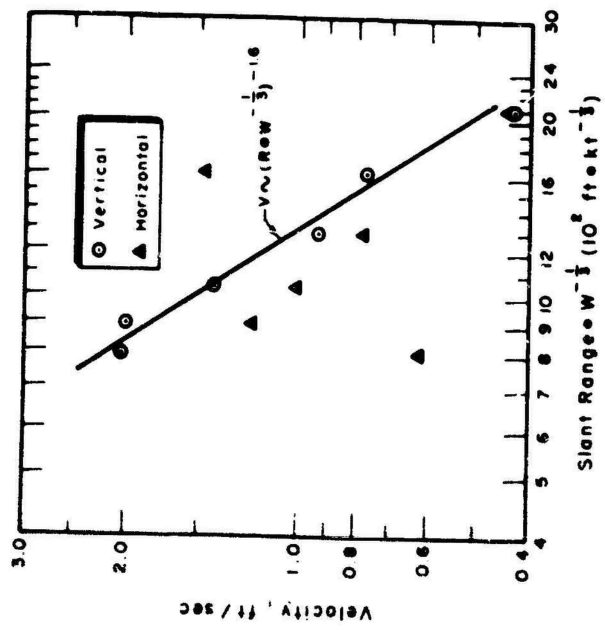


Figure 6.8 First peak horizontal and vertical velocity, surface level, Rainier.

**6.2.2 Particle Displacement.** A composite of the displacement-time (integrated acceleration) curves for the deep vertical hole is presented in Figure 6.9. The displacement at 320-foot depth is not the maximum displacement; the gage cable broke before zero velocity was attained. The curves of Figure 6.9 show a behavior similar to the particle velocity (see Figure 6.5).

It is of interest to compare the double integration of the OAPA acceleration record with the photographic data of earth motion near ground zero obtained by EG&G (Reference 13). This comparison is presented in Figure 6.10. The EG&G curve (dashed) is a best-fit curve constructed through the scatter of raw data; to fit a curve through the measured data the data were smoothed by an increment method. Looking at Figure 6.10, the general form and maxima of the two displacement-time curves agree well; they differ only in such details as arrival time and time of maximum displacement.

Using the displacement-time curves from all the mesa line stations, it is possible to construct the curves shown in Figure 6.11, which represent the approximate vertical elevation contours (above preshot levels) at various times after detonation (the vertical scale has been greatly expanded to give readable curves). The contours indicate that the most significant surface displacement occurred near Station 0, with the contours falling off abruptly out to about 500 feet. Also, the crack or break which was mentioned in connection with the acceleration records is corroborated by the obvious difference in vertical displacement between Stations 1 and 2 at about 0.3 second. However, close examination of the data shows that this difference in displacement is only about 0.75 inch; although this is much larger than can be ascribed to integration inaccuracies, it is so small that perhaps it was not observed by the shot photography. It is rather apparent from the figure that the chunk which contains Station 1 (450-foot ground range) would bottom before the piece containing Station 2 (Figures 5.2 and 5.3).

Also shown in Figure 6.11 is the normalized vertical displacement contour for the static case (see Appendix B). As one would expect, this static contour shows the displacement decaying with distance much more slowly than was observed on Rainier shot.

The first peak vertical displacement in the deep hole is plotted in Figure 6.12, and the initial decay of the peak follows the relation

$$(D \cdot W^{-1/3}) = 1.8 \times 10^{22} (R \cdot W^{-1/3})^{-8.5}, \quad (6.9)$$

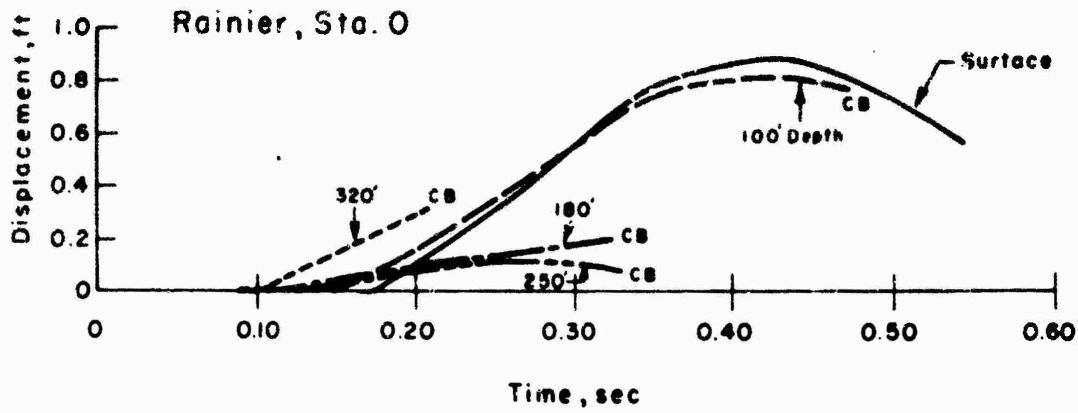


Figure 6.9 Earth displacement vs time, deep hole, Rainier. (CB - cable break.)

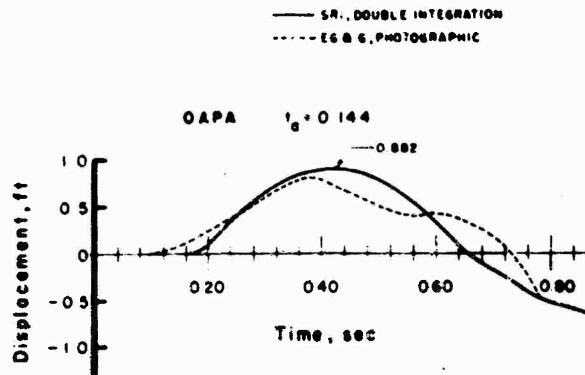


Figure 6.10 Comparison of ground zero displacement (EG&G) with SRI data.

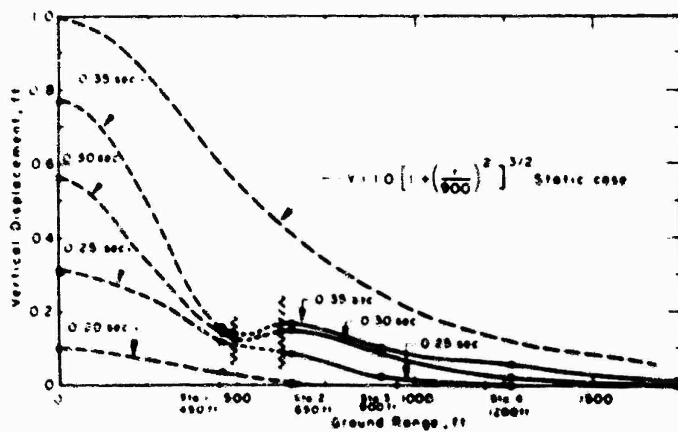


Figure 6.11 Vertical displacement contours at various times.

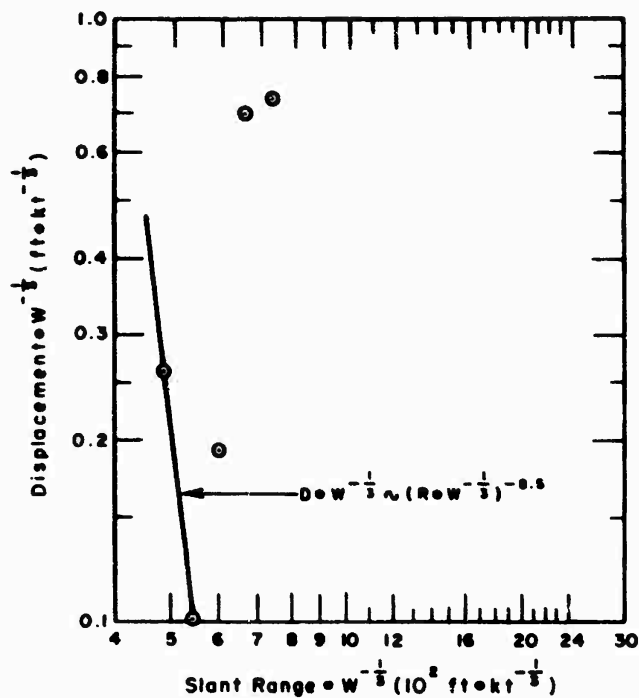


Figure 6.12 First peak vertical displacement, deep hole, Rainier.

where  $D$  and  $R$  are in feet and  $W$  is in kilotons. Again, one must be cautious about generalizing this result for prediction purposes, due to the particular layering of the Rainier mesa.

The peak displacements on the surface and slope lines are presented in Figures 6.13 and 6.14. The peak vertical displacements on the mesa obey the relation

$$(D \cdot W^{-1/3}) = 6.0 \times 10^3 (R \cdot W^{-1/3})^{-1.6} \quad (6.10)$$

And, it is obvious from the figure that, except for the station closest to ground zero, the peak horizontal displacements are larger than the corresponding vertical displacements. This result suggests that there was a tendency for the lifted cap rock to move up and away from surface zero at ground ranges beyond about 500 feet.

The slope line displacement data of Figure 6.14 indicates much higher (by a factor of 2 to 4) close-in peak displacements on the slope than on the surface. This confirms visual observations that the material on the slope was not as competent as that on the mesa surface.

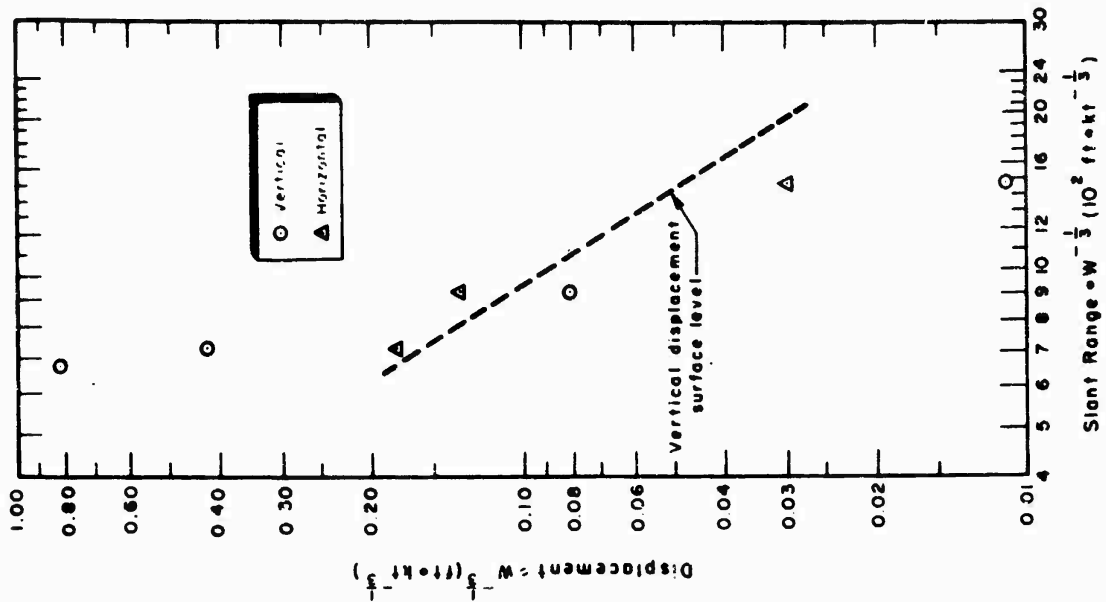


Figure 6.14 First peak horizontal and vertical displacement, slope line, Rainier.

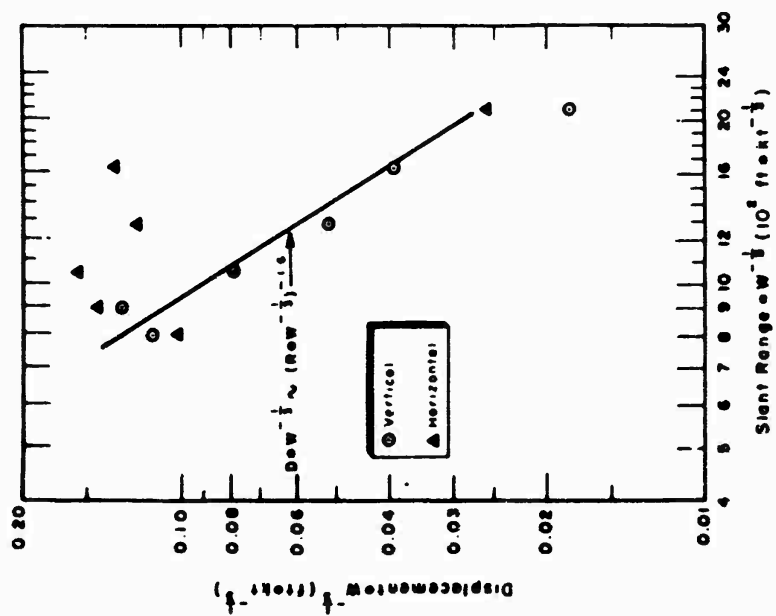


Figure 6.13 First peak horizontal and vertical displacement, surface level, Rainier.

TABLE 6.1 PERMANENT DISPLACEMENT AT SRI GAGE STATIONS, RAINIER.

Station	Ground range	Station radial plane <sup>a</sup>	Permanent horizontal displacement	Direction of horizontal motion <sup>a</sup>	Permanent vertical displacement	Direction of vertical motion
	ft	deg	ft	deg	ft	
1	458	225	0.45	42	0.14	down
2	655	225	0.33	39	0.02	down
3	902	225	0.18	41	0.01	up
4	1273	225	0.11	22	none	- -
5	1732	225	(No data obtained)			
6	2339	225	(No data obtained)			
10	481	126	0.37	3	0.43	up
11	600	162	0.24	87	0.50	down
12	881	182	1.05	300	0.57	up
13	1656	182	0.33	350	0.07	down

<sup>a</sup>The radial plane orientation of the station is taken from north as zero, positive clockwise.

Table 6.1 presents the permanent displacement data at the Project 26.4a mesa and slope gage stations obtained by survey after the Rainier event. The permanent motion measured on the mesa surface appears to exhibit the same general behavior as shown in Figure 6.13; that is, the horizontal displacement is much larger than the vertical movement at each station. Reference to the direction of the horizontal movement, with respect to the radial plane passing through the gage station and ground zero, confirms that at the closer ranges (Stations 1 and 2) the final displacement was down and in relative to preshot position. No such consistent behavior is observed on the slope line. The largest permanent displacements are observed at Station 12, where the final displacement is up and generally inward (about 60° off the trace radius). However, permanent displacement results at the other stations reveal both net upward and downward as well as outward movement, with no apparent consistency with respect to ground range.

### 6.3 SEISMIC PROPAGATION VELOCITIES

Velocities can be computed from the data obtained from the nuclear shot, as well as from the subsidiary prior seismic survey made by U.S.

**Geological Survey (USGS) (Reference 1).**

The survey performed by USGS was conducted by exploding charges at the bottom of a 100-foot hole and recording arrivals at various depths in a survey hole 200 feet away, and at points on the surface between the holes. Both holes were vertical. The survey hole was 800-feet deep, the top 400 feet was cased, and geophones were hung in the hole (air coupling). Since horizontal distance between the holes was but double that of the charge depth, many of the seismic rays were horizontal and most were slanted.

Anomalous velocities were obtained in this survey. Horizontally from shot point to survey hole, the velocity measured was 2600 ft/sec; slant velocities from shot point to shallower points in the survey hole were in the range 2600-2900 ft/sec. These velocities correspond to paths that deviate no more than 30° from horizontal.

The seismic rays travelled in more nearly vertical paths to those geophones which were on the surface, between the holes. The velocities measured were the greater the more nearly vertical were the paths; the measured velocities increased from 2900 to 3800 ft/sec. Unfortunately, no geophone was placed directly beside the shot hole. The survey therefore indicates fairly high differences between horizontal and vertical velocities in the rhyolite cap at points closer than 100 feet to the surface.

Rays which reached geophones 250 or more feet below the surface travelled in more nearly vertical paths. Again the results are not easy to interpret, since the composition (and therefore seismic velocity) changed greatly at a point about 265 feet down the survey hole. If the horizontal and vertical velocities at most points below the shot hole were equal (a question on which no evidence is available from this survey), the vertical velocities at various depths can be computed (Table 6.2 and Figure 6.15b). Some of these interval velocities were measured in the nuclear shot as is also shown.

**TABLE 6.2 INTERVAL VELOCITIES FROM USGS DATA**

<u>Depth</u>	<u>Interval velocity</u>	<u>Depth</u>	<u>Interval velocity</u>
ft	ft/sec	ft	ft/sec
230-270	7150	395-525	7070
270-310	13700	525-675	7180
310-395	6650	675-775	5850

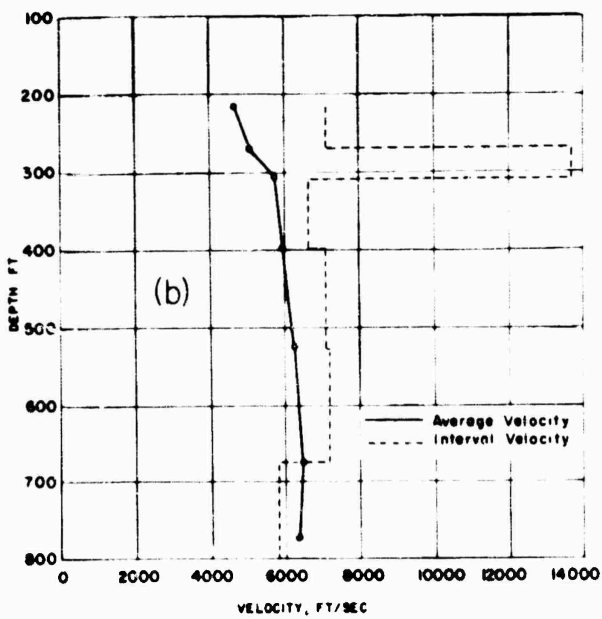
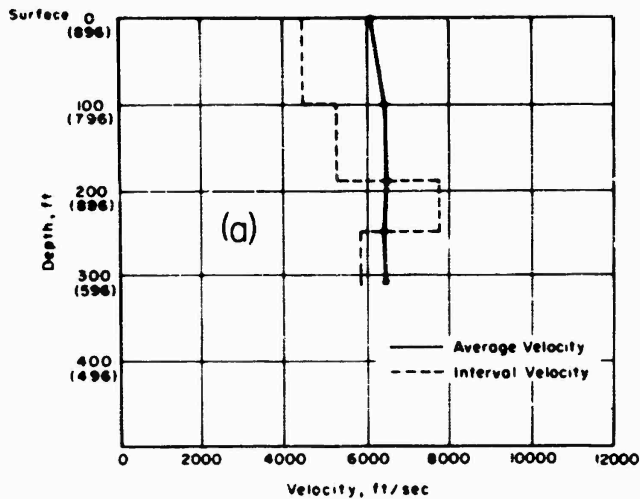


Figure 6.15 Velocity vs depth. (a) Rainier. (b) USGS Seismic Survey (preshot data).

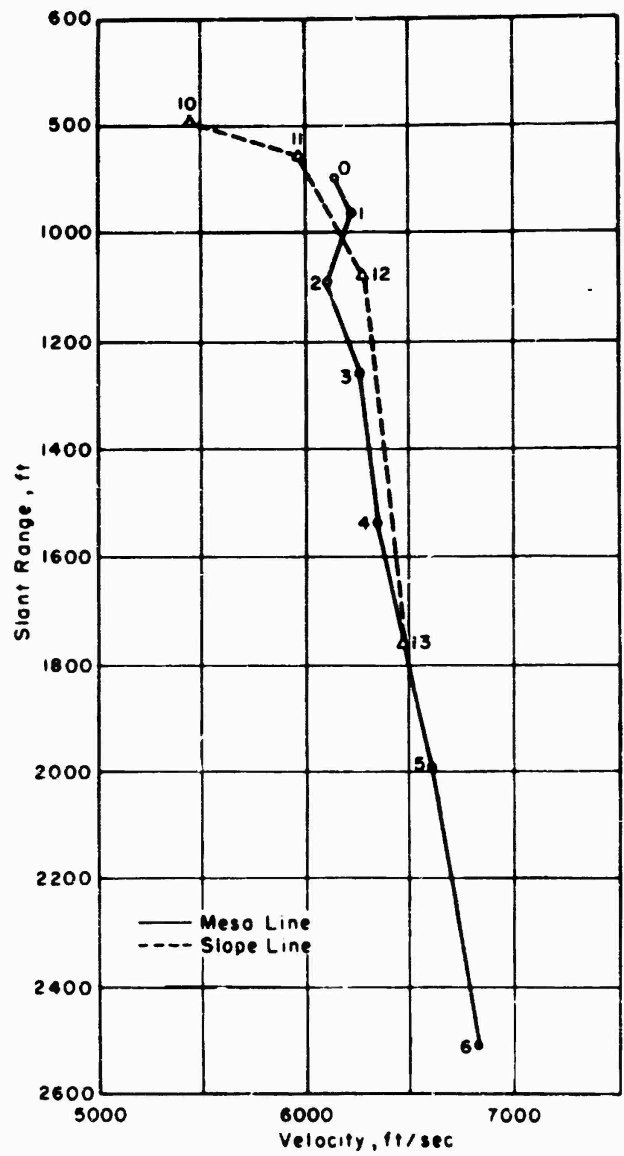


Figure 6.16 Velocity vs slant range, Rainier.

The stress wave from the center of the Rainier explosion travelled vertically to Station 0 and nearly vertically to Stations 1, 10, 11, 12, and 13, the last four on the slope line. Average velocities of the first pulse arrivals and interval velocities in the deep hole are shown in Table 6.3 and Figure 6.16. The first interval velocity (4500 ft/sec) in Table 6.3 is consistent with the USGS measurement of 3800 ft/sec for nearly vertical travel at the same point.

Average velocities to the distant stations (5 and 6) were somewhat greater than velocities to the others. Therefore, the seismic ray must have travelled a greater distance through a high-velocity layer to reach these stations. A clue to the location of this high-velocity layer is given in Figure 6.15, Table 6.2, and in the graph (Figure 6.17) of arrival times versus ground range.

TABLE 6.3 SEISMIC VELOCITIES, RAINIER

Station	Slant range	First arrival	Average velocity	Interval velocity	Arrival first peak	Average velocity	Interval velocity
	ft	msec	ft/sec	ft/sec	msec	ft/sec	ft/sec
OAP	889.5	144	6170		184	4830	
1AP	970.9	157	6230		185	5250	
2AP	1095	179	6120		209	5250	
3AP	1265	202	6260		226	5600	
4AP	1553	245	6340		281	5530	
5AP	1957	296	6600		356	5500	
6AP	2518	359	6820		419	6000	
OAP	889.5	144	6170		184	4830	
100	799.5	124	6450	4500	148	5400	2500
180	719.5	109	6600	5330	130	5540	4450
250	649.5	100	6495	7780	120	5410	7000
200	579.5	88	6590	5840	106	5460	5000
10AP	797.1	146	5460		170	4690	
11AP	860.4	144	5975		168	5150	
12AP	1084	173	6270		213	5100	
13AP	1774	274	6475		324	5480	
	<u>Ground range</u>						
1AH	458.4	157		9850	189		14000
2AH	654.8	177		9880	203		
3AH	901.7	202		8630	228		4810
4AH	1273	245		9780	305		8670
5AH	1732	296		9350	358		8800
6AH	2339	361			427		

The fact that all but one of the points on Figure 6.17 lie on a straight line suggests that the first arrivals travelled along an interface; that is, behaved as captured rays.

To check this idea, rough computations were made as follows. The hill was assumed to be composed of three layers with horizontal interfaces, and with the layers having the following depths and isotropic seismic velocities: 0 to 200 feet, 5000 feet per second; 200 to 300 feet, 10000 feet per second; and 300 to 900 feet, 6600 feet per second.

The refracted rays have been traced through the medium; Figure 6.18 shows their approximate shapes. Arrival times have been computed according to this figure. For a preliminary model, these computed arrival times show satisfactory agreement with the actual times.

Thus, it may be concluded that the medium is many-layered, with seismic velocities which are widely different in the different layers, and which do not increase monotonically with depth, and that rays to stations on the mesa are captured on a high-velocity interface (Figure 6.18). This latter conclusion is verified by the data on interval horizontal seismic velocities listed in Table 6.3. These data indicate velocities very close to the 10,000-ft/sec value as assumed in Table 6.3 and used in the computation of the arrival times. This confirms the assumption that energy is channeled through the higher velocity layers.

#### 6.4 EARTH STRAIN (SURFACE)

In general, the predicted strains were higher than those observed; therefore, most of the strain records are of low amplitude. The most notable exceptions to this are the horizontal strain records obtained on the slope (Stations 10 and 11, Figure 5.15); these records display large strain maxima occurring after the earth cap had apparently bottomed. Because visual observation at the time of detonation revealed much rock breakage and sliding down the face of the slope, the origin of these large strains on the slope is somewhat in doubt. As a matter of fact, the obvious increase in strain on the 10SH record before the break at 1.04 seconds may have been due to a rock hitting the wire span and breaking the strain wire.

It is worth noting that the horizontal strain-time records at Stations 2, 3, 4, and 5 (Figures 5.14 and 5.15) begin with negative (compressive) strains; this behavior is probably indicative of the compressive flexure which

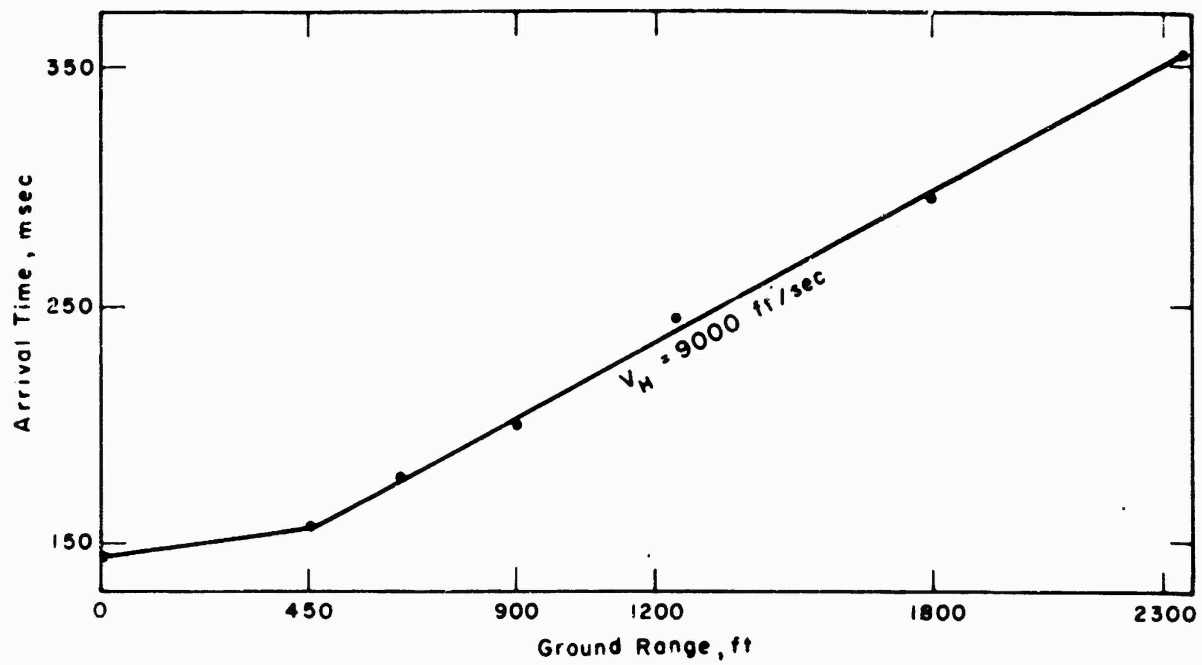


Figure 6.17 Arrival time vs ground range.

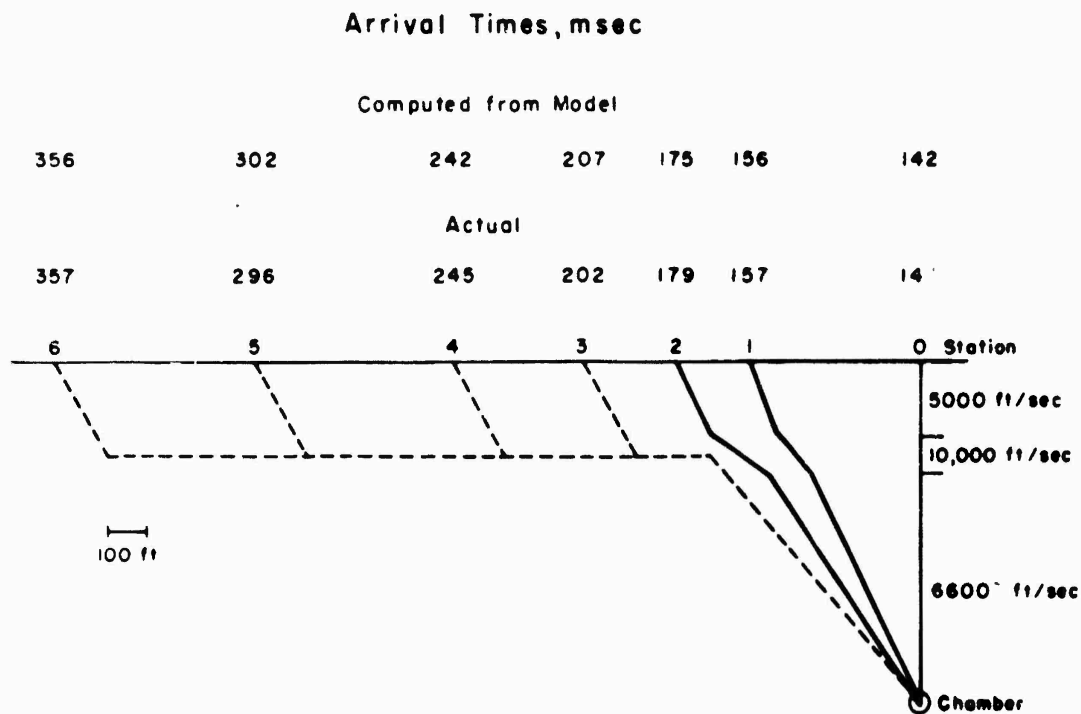


Figure 6.18 Schematic of seismic rays from chamber.

should occur at these stations before the general terrain rises and tensile strains are observed.

Figure 6.19 is a plot of the peak strain versus ground range for Rainier. Also included in the figure is the shape of the strain prediction curve (normalized to the average measured peak strain at Station 0). It is noted that the horizontal strain measurements, consistent with the acceleration results, indicate that the principal disturbance at the mesa surface was confined to a relatively small (less than 500-foot radius) region surrounding ground zero. Although the shape of the prediction curve is not unlike the observed curve, the latter does not indicate negative (compressive) peak strain at the mid-ranges. The residual strain data shown in Figure 6.19 indicate positive strains out to 900-foot radius and near-zero strains beyond. The peak strains measured on the slope line are significantly larger than would be expected at comparable ranges on the mesa, showing again that the material on the slope is probably less competent than that on the mesa.

As pointed out in Chapter 2, the transverse (OST) and horizontal (OSH) strain gages at Station 0 were laid out with a common reference point near ground zero; thus, in truth, both gages measured the radial component of strain. Comparison of the maximum positive strains on the two records (Figure 5.14) shows 3.46 ppk for OSH and 4.51 ppk for OST; this difference, if one assumes symmetrical motion radially from ground zero, could be accounted for by a preferential motion of the reference point of only 0.45 inch along the OSH radial direction. Nevertheless, a scatter of this magnitude is not surprising when one considers that several cracks appeared on the surface within the span of each of these gages. The rock simply would not support tensile strains of this magnitude.

With the data of Figure 6.19, it is possible to compute average earth strains at various depths in the deep hole by observation of the differences in displacement at the same time for two adjacent depths and dividing by the depth difference (Table 6.4). The average vertical strains are all computed at 0.200 second, which is before the estimated time of parting of the earth cap from the hill.

Table 6.4 shows that between 320- and 250-foot depths the average strain is the largest and compressive (negative), while between 250 and 180 feet the strain is tensile. The average strain is also tensile, but larger, between 180 and 100 feet, becoming compressive in the top 100 feet. The

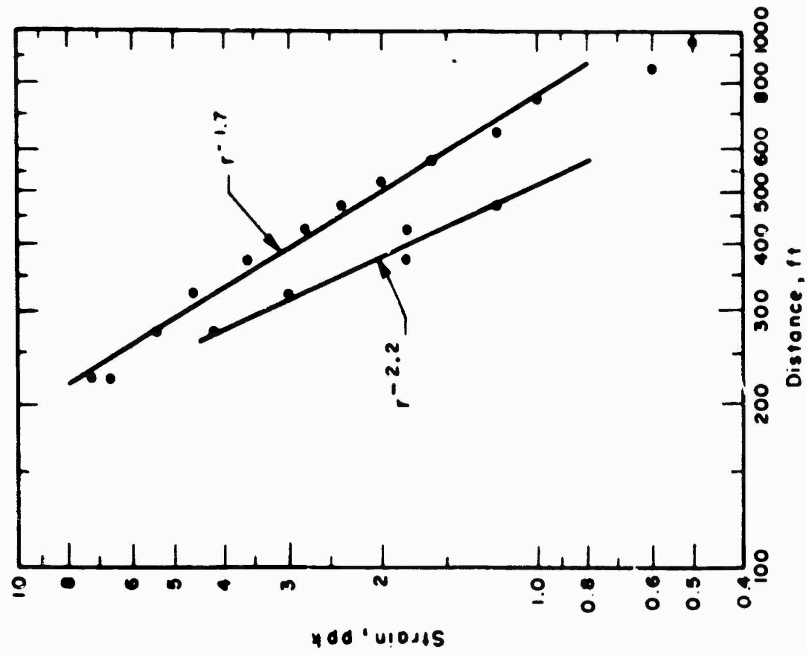


Figure 6.20 Residual strain, Rainier Tunnel, computed from permanent displacement.

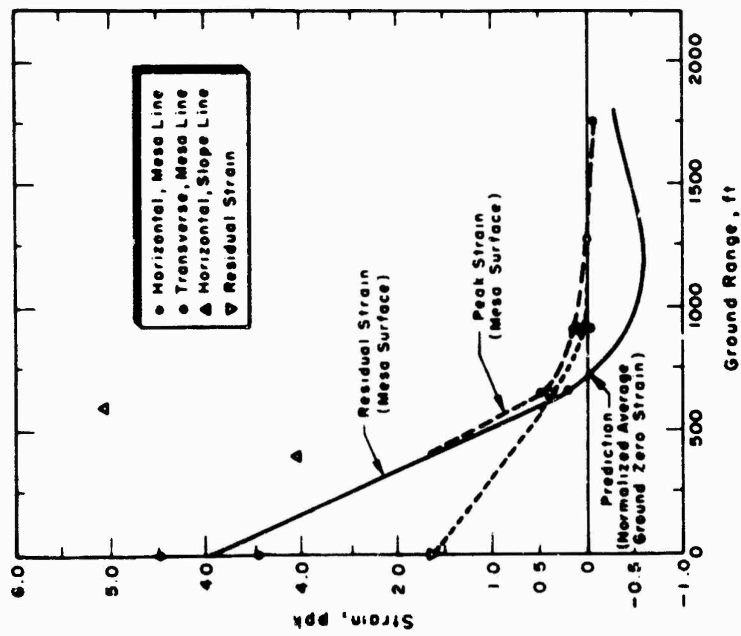


Figure 6.19 Earth strain, Rainier.

values of average tensile strain (0.26 and 0.9 ppk) are interesting in the light of experiments on tension failure of rock (Reference 14), which indicate strains at tension failure of about 0.1 ppk. However, it is significant that the field measurements of strain are controlled by the opening and closing of the joints and fractures in the rock. Hence, one should not expect that the measured strains will correlate with modulus or strain-at-failure data from laboratory tests on sound chunks of rock.

**TABLE 6.4 COMPUTED VERTICAL STRAIN IN DEEP HOLE, SHOT RAINIER**

Gage code	Depth of gage ft	Time of dis- placement sec	Displace- ment ft	Change in dis- placement ft	Span ft	Strain ppk
OAP320	320	0.200	0.301	-0.217	70	-3.1
OAP250	250	0.200	0.084	+0.018	70	+0.26
OAP180	180	0.200	0.102	+0.075	80	+0.9
OAP100	100	0.200	0.177	-0.071	100	-0.7

There is one final computation of strain which can be made; that is, using the permanent displacement data obtained in the Rainier tunnel, it is possible to calculate the average residual strain (horizontal) in the rock at distances from 200 to 1000 feet from the explosion (Figure 6.20). Although the relationship between the magnitude of average residual strain and the peak strain is not known, these calculations will give the approximate decay of strain with distance at close-in ranges to an underground nuclear detonation.

The data of Figure 6.20 appear to separate into two groups, in which the curves obey the relations:

$$\text{Strain (ppk)} = 9.5 \times 10^5 \gamma (\text{ft})^{-2.2}, \quad (6.11)$$

and

$$\text{Strain (ppk)} = 7.9 \times 10^4 \gamma (\text{ft})^{-1.7}. \quad (6.12)$$

These results are consistent with a large body of data obtained from high-explosive work in various rock types. Experimental field data for various rock types and explosives (Reference 15) indicate that the exponent of  $r$  varies from -2.5 to -1.6, which compares very well with the computed residual strains of Rainier (Figure 6.20).

## 6.5 APPLICABILITY OF PROJECT 26.4a INSTRUMENTATION

After a project of this type, it is pertinent to examine in retrospect the applicability of the experiment plan and the instrumentation as a guide for planning any future similar experiments.

6.5.1 Limitations of Plan. The limitations imposed upon earth velocity and displacement results by integrating acceleration-time records has been discussed previously (Section 5.2). Each time the data are integrated, accuracy is sacrificed; one can regard only the peak displacement values as reliable quantities.

The manner in which the gages on the slope had to be installed (on outcroppings) seriously limited the usefulness of these data for prediction of response from underground explosions.

Since so few surface strain measurements were made in the area near ground zero, where maximum motion occurred, these data are of limited use. However, this was the first test of its type, and the instrument plan had to contemplate possible strains of interest at a distance.

It is now apparent that it would have been desirable to obtain more data close to the explosion, just outside the hydrodynamic region. In the original plan, these measurements were omitted on the basis of time and cost, as well as in recognition of the hazard to the whole experiment of attempting to place these instruments.

The measurement of "permanent displacement" by surveying methods is useful, but it appears that there are probably relatively slow movements of the surface over a period of minutes, hours, or days after the shot. If these motions were measured, one might better understand the early phenomenon of cavity formation and subsequent collapse.

6.5.2 Limitations of Instrumentation. The major shortcoming of the performance of the instrumentation was the early cable failures of the subsurface gages. This was caused by an unanticipated phenomenon, the parting of the formation. The early damage to the gages on the slope was anticipated, but it could have been prevented only by a major effort.

6.5.3 Suggested Improvements. The following are suggestions for improving the overall usefulness of data obtained on any future test of this

**general type:**

a. A gage should be developed for measuring earth particle velocity as a function of time, as an adjunct to or in place of the ubiquitous accelerometer.

b. Gage cables cemented in place should be of a type which will allow large strain, and preferably which will allow the conductors to slip inside the jacket, to avoid the breakage experienced on this project.

c. Study should be devoted to methods of placement and grouting which will allow placement at depth, and to gages and cable attachment which will have a good probability of survival at close-in regions.

d. Attempts should be made to measure the time and location of gross fractures in the interior of the formation.

e. A means should be devised to measure and record the postshot motions of the surface near ground zero over a time of several hours or days after the shot.

## CHAPTER 7

### CONCLUSIONS

#### 7.1 INSTRUMENTATION PERFORMANCE

All 34 instrument channels gave usable records although 4 were incomplete due to cable breaks. However, even on these 4 there was sufficient recording to allow definitive conclusions.

#### 7.2 ACCELERATION

Peak vertical acceleration measured in the deep hole decayed sharply with distance from the charge between the 250- and 320-foot stations. However, at 180-foot depth and above, peak acceleration deviated markedly from regular behavior until at the surface it was 4 times that at 250-foot depth. Only the peak acceleration at 320-foot depth was close to prediction. The severe decay of peak response with distance from the explosion and the abrupt increase at 100-foot depth were contrary to prediction, the former result being ascribed to the effect of the energy proceeding from a relatively soft material (tuff) to a harder rock (rhyolite).

The secondary upward acceleration observed at 100 and 180 feet is caused by the reflected stress wave traveling downward, with the tension peak lagging the compression peak by the length of time it takes a stress wave to travel to the surface and return. Since there is no peak identifiable with the reflected energy at the expected times at 250-foot depths, the earth may have parted somewhere below 180-foot depth.

Although it can be concluded that the depth at which the "cap lifting" fracture occurs will probably increase as the scale of the experiment increases, it does not follow directly that this can be used as a firm criterion for containment. From surface vertical acceleration records from ground (surface) zero to 900 feet it is concluded that the surface at these radii was thrown up and was in free fall for several tenths of a second. Horizontal acceleration data confirm this conclusion. Wave forms follow the general pattern of the record obtained at surface before the cables were broken.

Secondary acceleration pulses indicate that there must have been a severe fracture between surface zero and 450 feet (horizontal ground range) since two distinct bottomings were recorded.

At close-in ranges, the horizontal component of acceleration was markedly less than the vertical, and beyond 1200 feet (A-scaled range) the two components are more comparable. The differences between peak accelerations on the surface and on the slope are negligible. Decay of peak vertical acceleration with distance is similar for Rainier and Ripple Rock.

### 7.3 VELOCITY

Velocity records obtained by integrating accelerations evidence parting of the earth formation at a minimum of two depths, probably between 0 and 100-foot depths. Layering characteristics of the formation in which a device is detonated influence the severity of the ground motion. Rainier vertical velocity decays with slant range similar to that at Ripple Rock.

### 7.4 DISPLACEMENT

The general form and maxima of the surface-zero electronically-measured displacement (doubly-integrated acceleration) agree with that of photographically recorded displacement. The greatest displacement occurred near surface zero, with corroborating evidence of vertical fracture between 450 and 650 feet ground range.

Except for the station closest to surface zero, peak horizontal displacement is greater than the corresponding vertical displacements, suggesting that the cap rock moved up and away from surface zero beyond 500-foot ground range. Permanent displacement measured on the surface also exhibits greater horizontal than vertical movement at each station, with the final displacement downward and inward toward ground zero, relative to preshot position. To the contrary, on the slope line, the greatest permanent displacements are observed at Station 12 (881-foot ground range), and the final displacement is up and generally inward. At other stations on the slope line the displacement reveals no apparent consistency with ground range.

### 7.5 SEISMIC VELOCITIES

From the preshot seismic survey and average velocities computed from the nuclear shot, it can be concluded that the medium of Rainier mesa

is many-layered with seismic velocities that are widely different and which do not increase monotonically with depth, and that seismic rays to stations on the mesa were captured in a high-velocity layer extending from near the surface to between 200 and 300 feet below it.

## 7.6 STRAIN

Predicted strains were higher than those observed. Horizontal surface strain measurements support the evidence from acceleration measurements that the chief disturbance at the mesa surface was confined to a relatively small region (less than 500-foot radius) surrounding surface zero. Peak strains measured on the slope are significantly larger than expected at comparable ranges on the mesa, indicating that the material on the slope is probably less competent than that on the mesa. Computations of residual strain from the permanent displacement data reveal results which are consistent with a large body of data obtained from high-explosive work in rock.

## CHAPTER 8

### RECOMMENDATIONS

For strong motion measurements on future deep underground nuclear explosions, it is recommended that:

1. More complete documentation of effects near ground zero be obtained.
2. Attempts be made to devise a gage which measures earth velocity directly.
3. Attempts be made to measure stress (or pressure) and strong motion parameters at stations very close to the device chamber, preferably in the "crushed" zone.
4. Efforts be made to complete a preshot and postshot survey of the area surrounding surface zero.

## APPENDIX A

### THE MEDIUM OF RAINIER SHOT

According to USGS data, there are in the mesa area three general types of material. Of the total section, about 70 percent can be classified as typical tuff (volcanic ash), about 15 percent poorly consolidated tuff, and about 15 percent welded tuff (rhyolite). In the section above the Rainier charge typical tuff is absent, and welded tuff forms the top 35 percent of the section. (The USGS 10- and 50-ton HE shots were in typical tuff.)

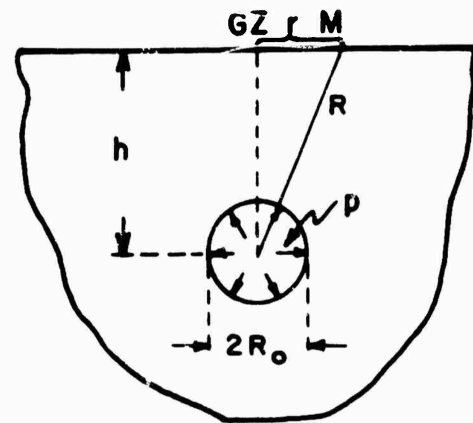
The three general types have the following characteristics: (Data was supplied by G. V. Keller, USGS.)

	<u>Typical tuff</u>	<u>Poor tuff (sand)</u>	<u>Welded tuff (rhyolite)</u>
Density	1.57 ± 0.16	1.6 ± 0.2	1.9 ± 0.2
Available porosity, average, percent	30	32	15
Total porosity, average, percent	45	40	35
Compressive strength, approximate	8600	2000 (est.)	high
Tensile strength	1000 (est.)	very small	1/9 compressive
Water content, percent	2-10	15-40	1-10

## APPENDIX B

### A NOTE ON PREDICTIONS FOR GAGE RANGE SETTING

At a depth  $h$  below the plane surface of a semi-infinite elastic medium a spherical bubble of pressure is introduced (see sketch D). If the radius of the bubble is small with respect to  $h$ , then the displacements of the surface at any point  $M$  after equilibrium is reached are as follows (from Reference 7). Vertical displacement (at ground range  $r$ ) =



Sketch D

$$w = 2(1-\sigma) \frac{C}{Gh^2} \left[ 1 + \frac{r^2}{h^2} \right]^{-3/2}$$

Radial displacement (at ground range  $r$ ) =  $u_r = \frac{r}{h} w$ ,

where  $\sigma$  = Poisson's ratio

$G$  = Rigidity modulus =  $E/2(1+\sigma)$

$E$  = Young's modulus

$r$  = ground range

$C = pR_0^3/2$

$p$  = pressure in bubble

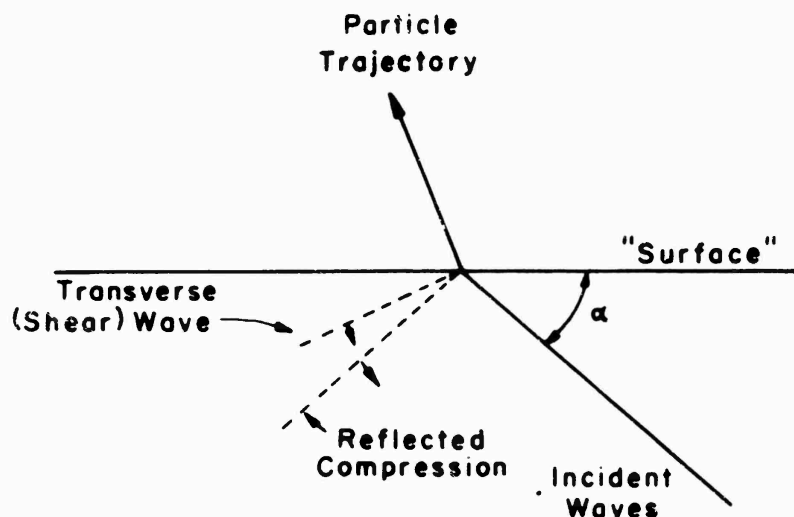
$R_0$  = radius of bubble

For the purpose of predicting ground motion, the true (or dynamic) solution was thought of as a perturbation of the solution of a static problem, in which the explosion center is replaced by a pressure center. In this model, straining but no yielding or fracture is assumed to occur.

There is another approach to the problem of predicting ground motion, which it is proper to mention briefly here. In this other method, each individual particle on the ground surface is assumed to detach itself individually from the medium as soon as the stress wave has been reflected from the

surface in the vicinity of that particle. This model is therefore a dynamic one; no doubt, it is much more dynamic than it should be. Quantitative results for this model have been obtained in an SRI report (Reference 10). The result is as follows (sketch E). If a plane wave is reflected from a surface, the particle velocity at a point P on the surface is about twice the particle velocity in an incident wave (less if the angle of incidence exceeds  $80^\circ$ , or if Poisson's ratio exceeds 0.3). The angle of emergence which the path of a freed particle would make with the original surface is twice the angle which the reflected shear wave makes with the surface.

Since this model was not used for prediction, no specific calculations based on it are included in this report.



Sketch E. Particle velocity due to reflection of a compression wave at the surface of an elastic medium.

## REFERENCES

1. Diment, W. H., and Dobrovolny, E., Feasibility of Proposed Underground Nuclear Test, USGS, 1957.
2. Vaile, R. B. Jr., Crater Survey, Proj. 3.2, SRI, Operation Castle, WT-920, 1955. Secret Restricted Data
3. Engineering Research Associates, Underground Explosion Test Program, TR 5-P-374, Sandstone, Vol. I, Feb. 15, 1953. Confidential
4. Salmon, V. and Doll, E. B., Ground Acceleration, Ground and Air Pressures for Underground Tests, Proj. 1.9a, SRI, Operation Buster-Jangle, WT-380, 1952. Secret Restricted Data
5. Swift, L. M. and Sachs, D. C., Underground Explosion Effects, Proj. 1.7, SRI, Operation Teapot, WT-1106, 1957.
6. Warner, Stanley, Surface Acceleration Measurements, USGS Tunnel, Room B, NTS, 5 April 1957, UCRL-4913, May 15, 1957. (Operation Plumbbob-Rainier)
7. Carrillo, Report on Subsidence in the Long Beach-San Pedro Area, SRI Report, May 1949.
8. Salmon, V., Air Pressure vs Time, Operation Tumbler, Proj. 1.2, SRI, WT-512, Feb. 1953. Secret Restricted Data
9. Salmon, V. and Hornig, S., Earth Acceleration vs Time and Distance, SRI, Operation Tumbler, WT-517, 1953. Confidential Restricted Data
10. Poncelet, E. F., Katz, S., and Fowles, G. R., Fundamental Studies of Small Cratering Charges (Foxhole Charges), SRI, Final report, Vol. II, Feb. 15, 1956.
11. Perret, W. R., Subsurface Motions from a Confined Underground Detonation--Part I, Operation Plumbbob, Proj. 26.4b, Sandia, WT-1529, 1958. Confidential
12. Wright, J. K., et al, "Observations on the Explosion at Ripple Rock," Nature, 182, 1597-98 (December 6, 1958).
13. Photographic Analyses of Earth Motion, Rainier, Operation Plumbbob, Proj. 26.4f EG&G, WT-1532, 1958.
14. Whitman, R. V., MIT, to D. C. Sachs, SRI, Private communication.
15. Duvall, W. I., "Strain Wave Shapes in Rocks Near Explosions," Geophysics, 18, 310-323 (April 1953).